Chapter 9 Tracer Transport in the Middle Atmosphere

9.1 Introduction: Types of Tracers

An atmospheric tracer may be defined as any quantity that "labels" fluid parcels. Tracers may be dynamical or chemical, conservative or nonconservative, passive or active. Dynamical tracers consist of derived field variables such as potential temperature and potential vorticity, which are conserved by fluid parcels under suitable conditions. Chemical tracers consist of minor atmospheric constituents that have significant spatial variability. All truly conservative chemical species are well mixed in the lower and middle atmosphere. Only species that have chemical sources and sinks (e.g., ozone) or that undergo phase changes in the atmosphere (e.g., H_2O) maintain significant spatial variability in the presence of the continual tendency for motions on all scales to keep the atmosphere well mixed below the homopause.

The single most important tracer for meteorologists is the potential temperature, defined in Eq. (1.1.9). For motions that are isentropic (i.e., adiabatic), fluid parcels must remain on constant potential temperature surfaces. Since potential temperature varies primarily in the vertical in the middle atmosphere (Fig. 9.1a) and is a monotonic function of height, it may be regarded as a vertical label for fluid parcels; for isentropic motion the problem of following fluid-parcel trajectories is reduced from three spatial dimensions to that of two-dimensional motion on the isentropic surfaces. Thus, the isentropic coordinates introduced in Section 3.8 are particularly useful in problems involving tracer transport.

Further constraints on fluid-parcel trajectories can be imposed by utilizing a second important dynamical tracer, Ertel's potential vorticity, P, defined

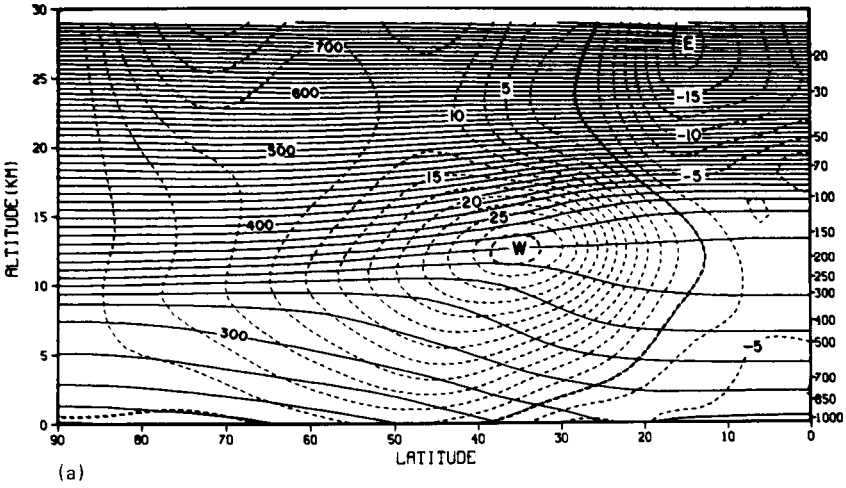

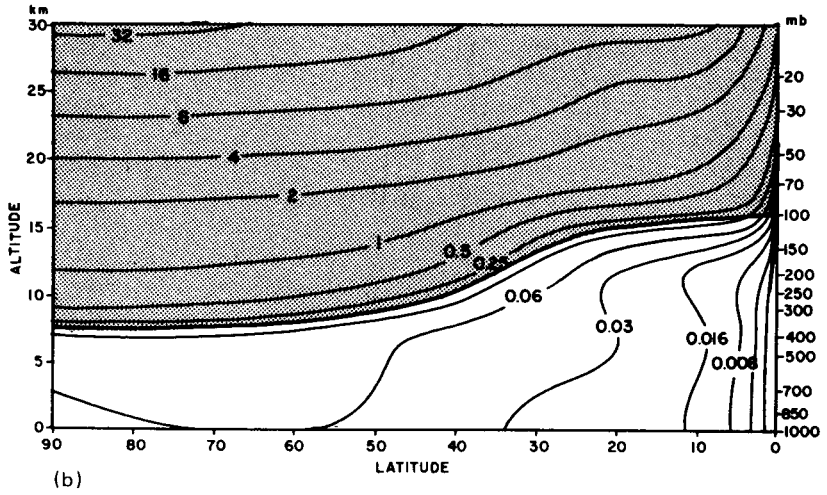

Fig. 9.1. Northern-Hemisphere zonal-annual mean cross sections for some quasi-conservative tracers. (a) Potential temperature (solid contours, kelvins) and zonal wind component (dashed contours, $m\,s^{-1}$). (b) Ertel potential vorticity in units of $10^{-5}\,K\,m^2\,kg^{-1}\,s^{-1}$. Area above the mean tropopause is shaded. (c) Ozone mixing ratio in parts per million by mass (ppmm). Shading extends from the mean tropopause to the level of maximum mixing ratio. Note that the tropopause [marked by heavy lines in panels (b) and (c)] intersects several of the potential temperature surfaces shown in panel (a). [From Danielsen (1985), with permission.]

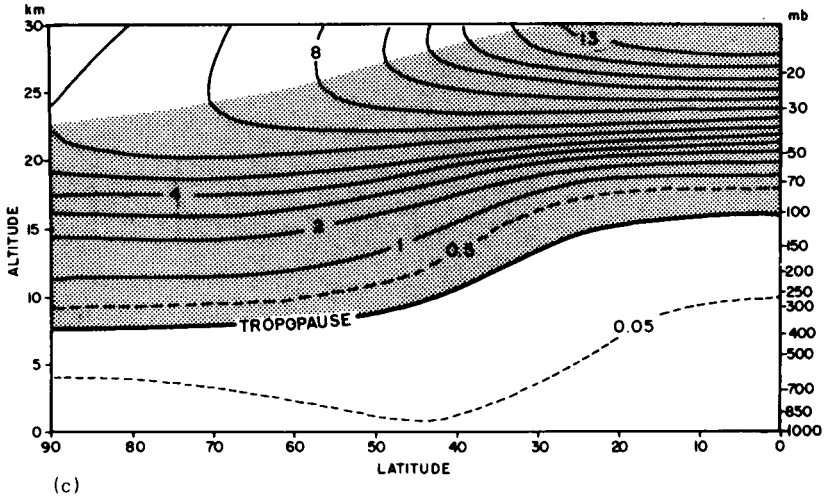

Fig. 9.1 (*continued*)

in Eqs. (3.1.4) and (3.8.4). Potential vorticity tends to vary strongly in both the meridional and vertical directions (Fig. 9.1b) and is conserved for adiabatic, frictionless flow. Thus, if it is assumed that the motion is adiabatic and inviscid, the contours of P on isentropic surfaces are material lines: that is, each contour always comprises the same fluid parcels. These material lines are generally wavy in shape, but tend to be oriented roughly in the east-west direction. The use of such contours in diagnosis of large-scale transport and mixing in the stratosphere was discussed in Sections 5.2.3 and 6.2.4.

Tracers are most valuable when they are conservative, so that their values remain constant following the motion of fluid parcels. In the atmosphere no tracer is truly conservative, since even in the absence of diabatic effects and chemical sources and sinks there will always be some mixing on scales smaller than the "parcel" resolved by a given measurement. It is useful, however, to distinguish those tracers whose rates of change following the motion are very small for the timescales of interest from those that change rapidly following the motion. The former will be referred to below as "quasi-conservative" or "long-lived" tracers. For motions on timescales of several days, the potential temperature and potential vorticity can be considered quasi-conservative tracers, as can ozone in the lower stratosphere (Fig. 9.1c). Thus, for example, since diabatic heating rates in the lower

stratosphere are generally less than 1 K day^{-1}, many months are required for the descent of a fluid parcel from the 30-km level (~800 K isentrope) to the 15-km level (~400 K isentrope), since a diabatic cooling of 400 K must occur. The rapid change of θ with height in the stratosphere, combined with the slowness of the diabatic heating or cooling, ensures that the vertical position of a fluid parcel can be followed quite accurately for several days, assuming isentropic motion. Of course, such parcels may move up and down a short distance (a few kilometers at most) with vertical displacements of the isentropic surface. Similar considerations hold for Ertel's potential vorticity. From Eq. (3.8.5), P is changed following the motion if there is a gradient of diabatic heating or if there is a nonconservative force such as friction or gravity-wave drag. In the stratosphere the timescale for friction appears to be comparable to that for diabatic heating, and both are of the order of weeks. Thus, both θ and P are excellent tracers for motions on timescales of less than a few weeks (as is ozone in the lower stratosphere). In the upper mesosphere, where gravity wave breaking reduces the frictional timescale to a day or so, P is no longer quasi-conservative.

The dynamical tracers θ and P are both "active" tracers in the sense that they are not simply passively advected by the flow field, but their distributions to a large extent determine the evolution of the flow field. This is especially true for the P field when it has large-scale structure.

An active tracer that is probably more familiar to meteorologists than the Ertel potential vorticity is the "quasi-geostrophic" potential vorticity, q_g. This quantity is conserved following the geostrophic motion on isobaric surfaces and is thus not an approximation to P (see Section 3.8). However, the stream function determining the geostrophic flow is defined in terms of q_g [see Eq. (3.2.15)], so that q_g not only is advected by the geostrophic flow but also determines it. Similar considerations apply to Ertel's potential vorticity, except that the advection is by the three-dimensional flow, and the distribution of P tends to determine the development of the flow in three dimensions (see Hoskins *et al.*, 1985.)

Chemical tracers may also be "active," albeit in a somewhat different sense. Thus, for example, chemical processes may change the ozone distribution, which changes the shortwave diabatic heating distribution, and hence changes the temperature and wind distribution. Other minor species involved in the photochemistry of the ozone layer may also play similar "active" roles, but these are for the most part quite small in the context of circulation changes.

For timescales of several weeks or less, ozone in the lower stratosphere may be considered a passive tracer for most purposes since ozone-induced changes in the circulation are usually second-order effects. For seasonal changes, however, the distribution of ozone is crucial to the determination

of the radiative forcing of the circulation. In turn, the circulation has important influences on the distribution of ozone. Passive chemical tracers can be of great value in identifying the history of air parcels. When insufficient data are available for accurate trajectory analyses, multiple chemical tracers can often be used to constrain the origins and trajectories of air parcels. This is especially useful for studies of troposphere–stratosphere exchange and transport within the lower stratosphere (see Section 9.6).

9.2 Long-Lived Chemical Tracers

Much can be learned about the overall mass flow in the middle atmosphere by considering the climatological distribution of quasi-conservative chemical tracers. The distribution of ozone, especially in the Northern Hemisphere, has been studied by balloon and ground-based methods for many years. However, only in the past decade, with the advent of routine satellite measurements, has it been possible to study its global climatology. For other long-lived tracers, such as methane (CH_4), nitrous oxide (N_2O), water vapor, and stratospheric aerosols, limited global measurements have been made by instruments on the *Nimbus* 7 research satellite. For less abundant species (e.g., various halocarbons), some information is available from balloon and aircraft measurements, primarily in midlatitudes.

The role of transport in determining the global distribution of chemical tracers depends on the nature and distribution of the tracer sources and sinks and on the relative magnitude of the timescales for dynamical and chemical processes. In the analysis of global transport it is useful to distinguish between substances whose sources are mainly in the troposphere and those whose sources are mainly in the stratosphere. The former, which include nitrous oxide, methane, and certain halocarbons, are slowly transported into the stratosphere, where they are destroyed by photolysis or oxidation. The latter, which include ozone, cosmogenic radionuclides (e.g., beryllium 7), and stratospheric aerosols, are transported slowly into the troposphere, where they are destroyed by a variety of processes.

The distribution of such substances in the stratosphere depends crucially on competition between dynamics and chemistry. This competition can be qualitatively measured by the ratio of the chemical and dynamical timescales. By "chemical timescale" we mean the characteristic time for replacement or destruction of a species by local sources or sinks. By "dynamical timescale" we are here referring to the time for advective processes (mean motions plus eddies) to transport the tracer through approximately a scale

height in the vertical or from equator to pole meridionally. Three cases can be distinguished:

1. The chemical timescale is much less than the dynamical timescale. In this case the species is in local photochemical equilibrium, and transport does not enter directly into the conservation equation for the species. Of course, transport may enter indirectly by affecting the concentration of other species that participate in the photochemical production or loss for the species in question. (See Chapter 10 for further discussion.)

2. The chemical timescale is much greater than the dynamical timescale. In this case the tracer is passively advected and in the absence of localized sources or sinks will eventually become well mixed due to the dispersive effects of transport. The rapid transport and long chemical time constants in the troposphere for species like methane and nitrous oxide are reflected by their uniform tropospheric distributions.

3. Chemical and dynamical time constants are of the same order of magnitude. This is the most interesting case (also the most difficult to handle), since the distribution of such species is determined both by chemistry and by transport. The distributions of methane and nitrous oxide in the meridional plane in the upper stratosphere are examples of species distributions that depend equally on transport and chemistry.

Figure 9.2 shows profiles of photochemical timescales at 30° latitude and equinoctial conditions for the tropospheric source species whose midlatitude

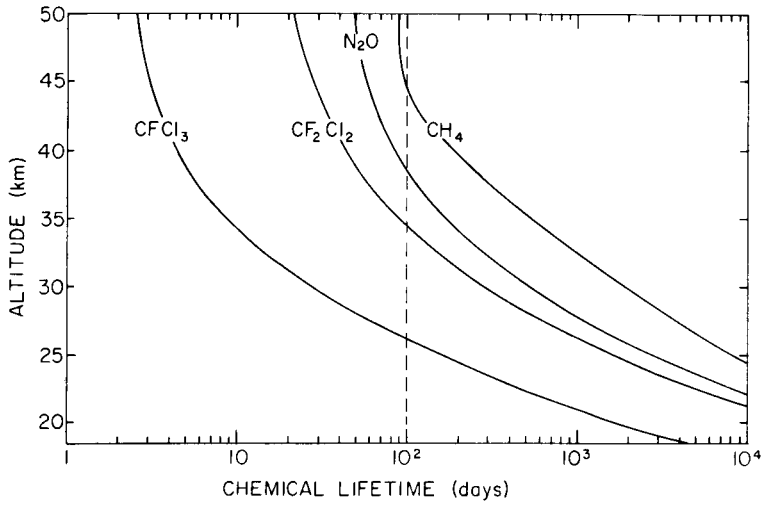

Fig. 9.2. Altitude dependence of lifetimes (i.e., *e*-folding decay times) for several long-lived trace gases at 30°N and equinoctial conditions calculated with observed ozone and 1983 chemistry. (Courtesy of Dr. J. A. Logan and Dr. M. J. Prather.)

vertical profiles were shown in Fig. 1.8. Methane is primarily destroyed through oxidation by reaction with the hydroxyl radical or through reaction with excited atomic oxygen or chlorine. Nitrous oxide and the chlorofluoromethanes are destroyed through photolysis by ultraviolet radiation. In all cases the destruction rates increase with height in the middle atmosphere. The mean concentration at any altitude results from a balance between the local destruction and the net convergence of the upward flux. Thus the species with the shortest chemical timescales have concentrations decreasing most rapidly with height.

The influence of transport on the long-lived tropospheric source gases can best be illustrated by considering their distributions in the meridional plane. Examples of monthly means for N_2O and CH_4 from the observations of the SAMS satellite experiment are shown in Fig. 9.3. The mixing-ratio surfaces for both tracers are bulged upward in the tropics and tend to slope downward toward the poles in both hemispheres, although there are important seasonal shifts in the latitude of the bulge and a double bulge occurs during Northern-Hemisphere spring. Recalling from Fig. 9.1 that isentropic surfaces have relatively small slopes in the stratosphere, it is clear that in general the isolines of constant mixing ratio for N_2O and CH_4 slope downward toward the poles more steeply than the isentropes, so that concentration decreases toward the poles on isentropic surfaces.

9.3 Transport in the Meridional Plane

Discussion of the processes through which the general circulation partly determines the observed meridional and vertical distributions of various tracers has often centered on the relative roles of "mean" and "eddy" motions. But, as indicated in Sections 3.5–3.7 and 3.9, the partitioning between mean flow and eddies depends critically on the type of averaging process used. The conventional isobaric Eulerian zonal mean, the transformed Eulerian mean (TEM), the generalized Lagrangian mean (GLM), and the isentropic zonal mean all generally provide different interpretations of "mean flow" and "eddy."

The relative importance of "mean flows" and "eddies" in transport is thus a difficult issue to resolve, even conceptually. One approach would be to compare observed tracer distributions with those obtained in a model that excludes eddy motions altogether (see Section 7.2.2). In such a model the temperature would generally be very close to radiative equilibrium; only the time dependence imposed by the annual cycle in solar heating would drive departures from radiative equilibrium. The flow would then be almost

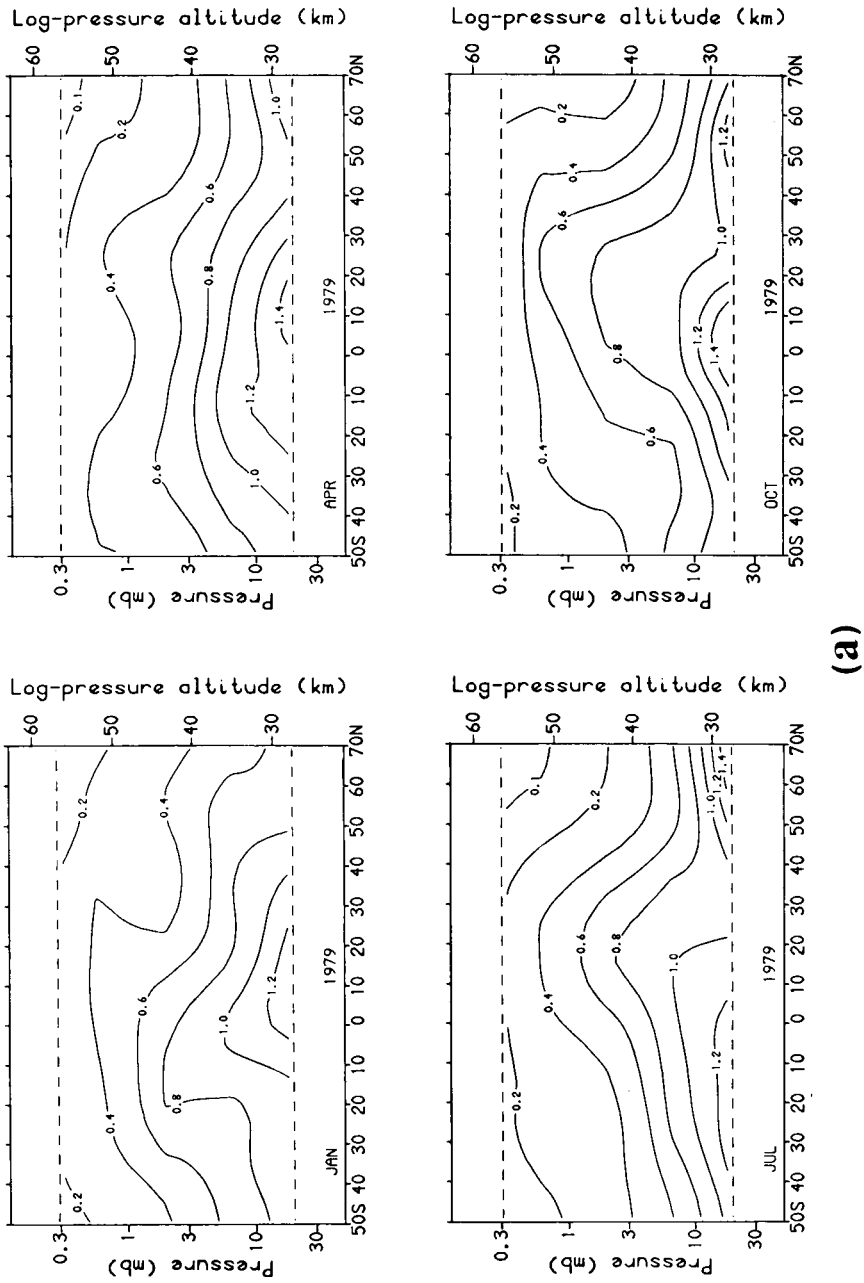
Log-pressure altitude (km)
Pressure (mb)
APR
1979
OCT
1979
JAN
1979
JUL
1979
50S 40 30 20 10 0 10 20 30 40 50 60 70N

(a)

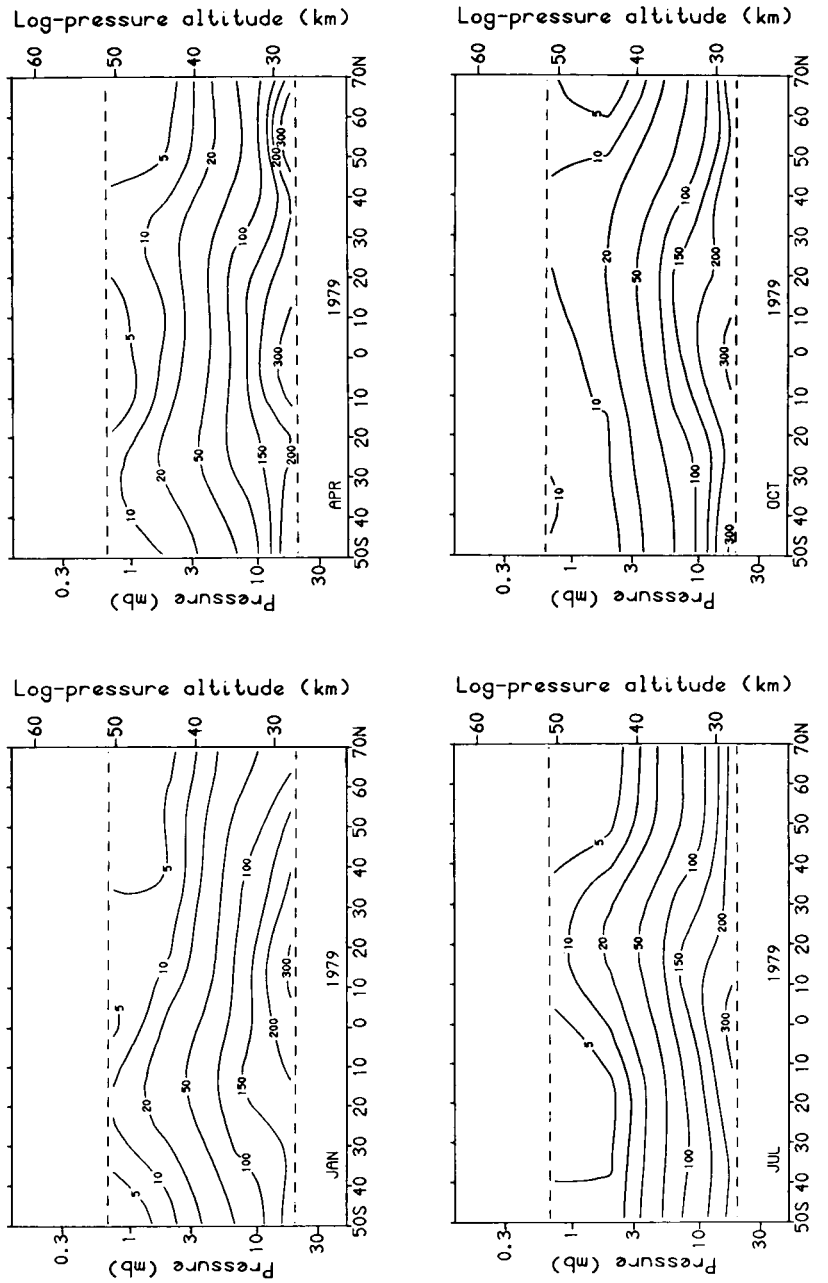

(b)

Fig. 9.3. Monthly mean cross sections of (a) CH_4 (ppmv) and (b) N_2O (ppbv) from measurements by the *Nimbus* 7 SAMS experiment during 1979. [After Jones and Pyle (1984).]

purely zonal and in thermal wind balance with the radiative equilibrium temperature distribution [Eq. (7.1.1)]; very little meridional transport would occur.

Thus, the circulation in the meridional plane should be regarded as primarily an *eddy*-driven circulation no matter how the actual flow is mathematically partitioned between "eddy" and "mean" portions. Rather than regarding the meridional transport as an eddy versus mean-flow problem, it is sometimes perhaps more sensible to separate bulk advection from diffusion, while recognizing that eddies directly or indirectly are the primary agents for both advective and diffusive transport.

9.3.1 Mean Transport: The Brewer–Dobson Model

The simplest qualitatively plausible model that can explain the gross characteristics of the stratospheric meridional distributions of tracers like N_2O and CH_4 consists of advection by a single mean meridional cell in each hemisphere with uniform rising motion across the tropical tropopause, poleward drift in the stratosphere, and, by continuity of mass, a return flow into the troposphere in the extratropics, as indicated schematically in Fig. 9.4. Such a circulation was proposed by Brewer (1949), who argued that "freeze drying" of air by upward motion through the "cold trap" of the high cold tropical tropopause seemed to be required to explain the observed low water-vapor mixing ratios in the stratosphere. Somewhat later, Dobson (1956) pointed out that poleward and downward advection by this type of mean circulation was qualitatively consistent with the observed high concentration of ozone in the lower polar stratosphere, far from the region of photochemical production. Although this "Brewer–Dobson cell," as it has come to be called, provides a partial model for the overall transport in the stratosphere, it does not by any means represent a complete physical description.

Part of the difficulty with the Brewer–Dobson model is purely conceptual. Since the meridional circulation of this model is derived from consideration of tracer transport, it must be regarded as a *mass* circulation, and hence closely related to the Lagrangian mean flow (see Section 3.7). However, meteorologists have tended in the past to interpret the Brewer–Dobson circulation as though it were an Eulerian mean meridional circulation. Thus, the model fell out of favor when diagnostic studies of the general circulation revealed that the observed Eulerian mean circulation in the winter stratosphere had a two-cell structure, with rising motion in both the tropics and polar latitudes and sinking in midlatitudes. In addition, observational studies of the transport of ozone and radioactive tracers in the lower

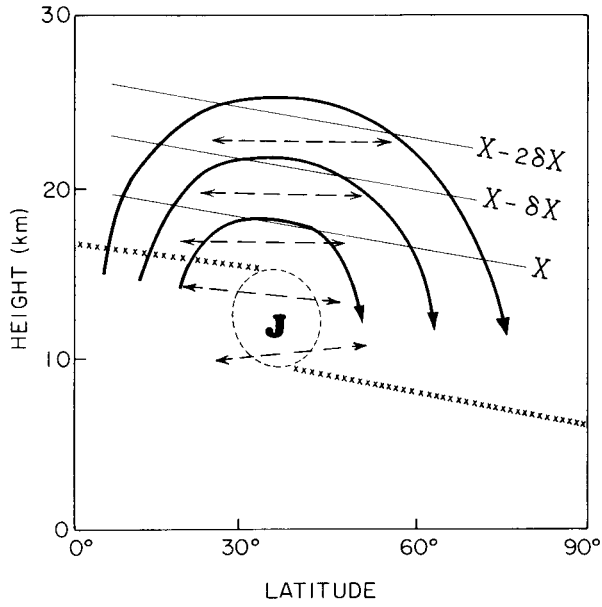

Fig. 9.4. Schematic cross section of transport in the stratosphere. Heavy lines show the mean meridional mass circulation (Brewer-Dobson cell). Dashed lines indicate quasi-isentropic mixing by large-scale eddies. The mean tropopause is indicated by crosses, and J indicates the mean jetstream core. Light lines labeled with mixing-ratio values (X) show mean slope of a long-lived vertically stratified tracer. [After Holton (1986b).]

stratosphere revealed that large-scale eddy motions play an important role in meridional and vertical transport, and that there often tends to be almost complete cancellation between Eulerian eddy and mean-flow transports.

Dunkerton (1978) used an approximate version of the GLM theory reviewed in Section 3.7 to show that the Brewer-Dobson cell should be interpreted as a Lagrangian mean circulation, not an Eulerian mean. He further suggested that the Lagrangian mean could be approximated by the residual circulation of the TEM equations introduced in Section 3.5, which is itself approximately equal to the "diabatic" circulation (see Section 7.2.3). The diabatic circulation is defined simply as the mean meridional circulation for which the adiabatic heating due to the mean vertical motion just balances the diabatic heating associated with the observed zonal mean temperature field: it was illustrated schematically in Fig. 7.2. Because the lower stratosphere is radiatively heated in low latitudes and radiatively cooled at high latitudes, the lower-stratosphere diabatic circulation in the meridional plane should have a structure similar to that of the circulation postulated by Brewer and Dobson (see the lower part of Fig. 7.2).

The mean distribution of a long-lived tracer implied by the process of advection by the diabatic circulation is qualitatively consistent with the observed distributions of N_2O and CH_4, in that surfaces of constant mixing ratio are bulged upward in low latitudes and slope downward toward the poles, as would be expected with upward advection at low latitudes and downward advection at high latitudes. The observed slopes of the mixing-ratio surfaces are, however, substantially less than would occur if the only processes operating were advection by the diabatic circulation and chemical destruction. Thus, the diabatic circulation is not an adequate quantitative model for the total eddy-driven transport.

9.4 Formulations of Eddy and Mean-Flow Transport

The discussion of the previous section suggests that conventional Eulerian averaging may not be a very efficient method of representing the physics of mean tracer transport in the meridional plane in the presence of large scale wave disturbances. In this section we examine various alternative schemes, some of which provide important insights into the influence of large-scale waves on net transport.

9.4.1 The Eulerian Mean Formulation and the Effective Transport Velocity

We start from the continuity equation for tracer mixing ratio:

$$D\chi/Dt = S, \tag{9.4.1}$$

where S, the net source, designates the sum of all production and loss processes. In the atmosphere the "source" represented by S must include not only chemical production and loss (see Appendix 10A), but also the effects of turbulent diffusion by the unresolved scales of motion. For this reason alone, tracers are never exactly conserved in observational analyses of atmospheric data. However, if the resolved scales include most of the tracer variance, the diffusive source can in many cases be neglected. Note that Eq. (9.4.1) is also the form of the conservation equations [Eqs. (3.1.3e) and (3.1.5)] for θ and P, with S suitably defined.

With the aid of the continuity equation [Eq. (3.1.1d)] we can write Eq. (9.4.1) in flux form as

$$(\rho_0\chi)_t + (\rho_0 u\chi)_x + (\rho_0 v\chi)_y + (\rho_0 w\chi)_z = \rho_0 S, \tag{9.4.2}$$

where for simplicity we use Cartesian coordinates. Averaging zonally and using Eq. (3.3.2d) yields the conventional Eulerian mean transport equation,

$$\bar{\chi}_t + \bar{v}\bar{\chi}_y + \bar{w}\bar{\chi}_z = \bar{S} - \rho_0^{-1}\nabla\cdot(\rho_0\overline{\mathbf{u}'\chi'}). \tag{9.4.3}$$

Note that the form of Eq. (9.4.3) is identical to that of the Cartesian coordinate version of the Eulerian mean thermodynamic equation [Eq. (3.3.2e)] when the eddy flux is written in vectorial form.

It was mentioned in Section 9.3 that a hypothetical middle atmosphere containing no eddies would be close to radiative equilbrium, with very weak meridional motions and tracer transport. If $\bar{S}$ were small, then $\bar{\chi}_t$ would also be small, by Eq. (9.4.3). The effect of eddies is to provide not only an eddy flux on the right of Eq. (9.4.3) but also a mean meridional circulation $(\bar{v}, \bar{w})$. These two terms are frequently found to cancel each other, to some extent (see Section 11.4, especially Fig. 11.10). For example, when averaged over a few weeks the tendency term $\bar{\chi}_t$ becomes small; if $\bar{S}$ is small, then the "mean advection" and "eddy" terms in Eq. (9.4.3) must almost balance. The determination of the *net* meridional transport due to the presence of eddies, and thus the calculation of $\bar{\chi}_t$, therefore involves careful consideration. It will be shown in Section 9.4.2 that this net transport, like the eddy-driven mean acceleration (see Section 3.6), depends on departures from steady, linear, conservative wave motion.

The role of eddies in transport of tracers can be elucidated by considering linearized disturbances $[\chi' = O(\alpha)]$ to almost zonal flow $[\bar{v}, \bar{w}, \bar{Q}, \bar{S} = O(\alpha^2)]$, where α is a measure of the eddy amplitude. Equation (9.4.1) shows that χ' satisfies the linear disturbance equation

$$\bar{D}\chi' + \mathbf{u}' \cdot \nabla\bar{\chi} = S' + O(\alpha^2), \tag{9.4.4}$$

where $\bar{D} \equiv \partial/\partial t + \bar{u}\,\partial/\partial x$. Defining parcel displacements (η', ζ') such that

$$\bar{D}(\eta', \zeta') \equiv (v', w') \tag{9.4.5a}$$

[cf. Eq. (3.7.1)] and a source term γ' such that

$$\bar{D}\gamma' \equiv S', \tag{9.4.5b}$$

we obtain from Eq. (9.4.4)

$$\chi' + \boldsymbol{\xi}' \cdot \nabla\bar{\chi} = \gamma', \tag{9.4.6}$$

where $\boldsymbol{\xi}' = (\xi', \eta', \zeta')$ is the parcel displacement vector.

Eliminating χ' in Eq. (9.4.3) with Eq. (9.4.6) we get, after some manipulation,

$$\bar{\chi}_t + \bar{v}^\dagger\bar{\chi}_y + \bar{w}^\dagger\bar{\chi}_z = \bar{S}^\dagger + \rho_0^{-1}\nabla \cdot (\rho_0 \mathbf{K}^{(s)} \cdot \nabla\bar{\chi}) + O(\alpha^3). \tag{9.4.7}$$

In Eq. (9.4.7) $\mathbf{K}^{(s)}$ is the symmetric "diffusion" tensor

$$\mathbf{K}^{(s)} \equiv \begin{bmatrix} K_{yy} & K_{yz} \\ K_{yz} & K_{zz} \end{bmatrix} \equiv \tfrac{1}{2}\begin{bmatrix} (\overline{\eta'^2})_t & (\overline{\eta'\zeta'})_t \\ (\overline{\eta'\zeta'})_t & (\overline{\zeta'^2})_t \end{bmatrix}, \tag{9.4.8}$$

a measure of the dispersion of parcels in the meridional plane (subscripts y and z in the components of $\mathbf{K}^{(s)}$ do not represent partial derivatives). Moreover, $(\bar{v}^\dagger, \bar{w}^\dagger)$ is the *effective transport velocity* (Plumb and Mahlman, 1987) defined by

$$\bar{v}^\dagger \equiv \bar{v} + \rho_0^{-1}(\rho_0\Psi)_z, \qquad \bar{w}^\dagger \equiv \bar{w} - \Psi_y, \tag{9.4.9a}$$

where

$$\Psi \equiv \tfrac{1}{2}(\overline{v'\zeta'} - \overline{w'\eta'}). \tag{9.4.9b}$$

is a stream function in the meridional plane.

From Eqs. (9.4.9a,b) and the Cartesian equivalent of Eq. (3.3.2d), it follows that

$$(\rho_0\bar{v}^\dagger)_y + (\rho_0\bar{w}^\dagger)_z = 0. \tag{9.4.9c}$$

Moreover,

$$\bar{S}^\dagger \equiv \bar{S} - \rho_0^{-1}\,\boldsymbol{\nabla}\cdot(\rho_0\overline{\mathbf{u}'\gamma'}) \tag{9.4.9d}$$

is a modified Eulerian mean source term. Noting that

$$\overline{v'\gamma'} = (\overline{\eta'\gamma'})_t - \overline{\eta' S'}, \qquad \overline{w'\gamma'} = (\overline{\zeta'\gamma'})_t - \overline{\zeta' S'},$$

we find that if the eddy tracer source is a weak linear relaxation so that $S' = -A\chi'$, and $|A\chi'| \ll |\bar{D}\chi'|$, then

$$S' \approx A\boldsymbol{\xi}'\cdot\boldsymbol{\nabla}\bar{\chi} \tag{9.4.9e}$$

and Eq. (9.4.9d) yields

$$\bar{S}^\dagger = \bar{S} - \rho_0^{-1}\,\boldsymbol{\nabla}\cdot(\rho_0\overline{\boldsymbol{\xi}'\gamma'})_t + \rho_0^{-1}\,\boldsymbol{\nabla}\cdot(\rho_0\mathbf{K}^{(c)}\cdot\boldsymbol{\nabla}\bar{\chi}) + O(A^2\alpha^2) + O(\alpha^3), \tag{9.4.10}$$

where

$$\mathbf{K}^{(c)} \equiv A\begin{bmatrix} \overline{\eta'^2} & \overline{\eta'\zeta'} \\ \overline{\eta'\zeta'} & \overline{\zeta'^2} \end{bmatrix}. \tag{9.4.11}$$

The tensor $\mathbf{K}^{(c)}$ is sometimes referred to as the "chemical diffusion" tensor. Notice that while $\mathbf{K}^{(s)}$ depends on the *rate of increase* of the mean square displacement, $\mathbf{K}^{(c)}$ depends on its amplitude and the tracer relaxation rate.

The complete Eulerian mean tracer transport equation [Eq. (9.4.7)] for linearized disturbances is rather complicated. However, for linear, steady, conservative ($A = 0$) waves, Eq. (9.4.7) simplifies to

$$\bar{\chi}_t + \bar{v}^\dagger\bar{\chi}_y + \bar{w}^\dagger\bar{\chi}_z = \bar{S}; \tag{9.4.12}$$

thus, in this particular case, the eddy effects are entirely incorporated in the effective transport velocity $(\bar{v}^\dagger, \bar{w}^\dagger)$.

An alternative formulation of the Eulerian mean tracer transport equation can be obtained by using the TEM formalism introduced in Section 3.5. Using the residual mean flow as defined by Eq. (3.5.1) we can rewrite Eq. (9.4.3) in the form

$$\bar{\chi}_t + \bar{v}^*\bar{\chi}_y + \bar{w}^*\bar{\chi}_z = \bar{S} + \rho_0^{-1}\nabla \cdot \mathbf{M}. \tag{9.4.13}$$

Unlike the effective transport formulation of Eq. (9.4.7), the residual mean form usually does not completely separate advective and diffusive effects of the eddies since $\mathbf{M}$ (defined in Appendix 9A) generally makes a contribution to the total advective transport. The difference between the effective transport circulation and residual circulation [see Eq. (9A.4)] is, however, usually small in the stratosphere. In Appendix 9A it is shown that if the waves are *linear*, *steady*, and *adiabatic*, then

$$\bar{v}^\dagger = \bar{v}^* \qquad \text{and} \qquad \bar{w}^\dagger = \bar{w}^*.$$

If in addition the tracer eddy is conservative ($\gamma' = S' = 0$), then $\mathbf{M} = (0, 0)$ and the TEM transport equation is identical to the form of Eq. (9.4.12). If furthermore the mean frictional and diabatic terms $\bar{X}$, $\bar{Y}$, $\bar{Q}$ all vanish, and suitable boundary conditions are imposed, then the nonacceleration theorem of Section 3.6 holds. Normally the mean flow then has $\bar{v}^* = \bar{w}^* = 0$ and the TEM transport equation reduces to $\bar{\chi}_t = \bar{S}$. The mean tracer tendency is due only to mean sources and sinks, and no net meridional transport occurs. This is called a *nontransport theorem.* For the same conditions the eddy flux divergence term on the right side in Eq. (9.4.3) will normally not vanish, but will be exactly balanced by mean advection due to the $(\bar{v}, \bar{w})$ field, which is also nonzero in this case. Thus, the TEM formulation of Eq. (9.4.13) or the effective transport formulation of Eq. (9.4.7) can be more efficient than the conventional formulation [Eq. (9.4.3)] for computing the evolution of a chemically active tracer under approximate nonacceleration conditions.

9.4.2 The GLM Formulation

Conceptually, the simplest framework in which to view the actual mass transport in the meridional plane is by use of the generalized Lagrangian mean (GLM) introduced in Section 3.7. In this approach, Eq. (9.4.1) is averaged along a wavy material tube of particles (see Fig. 3.1) and the mean equation has the form

$$\frac{\partial \bar{\chi}^L}{\partial t} + \bar{v}^L\frac{\partial \bar{\chi}^L}{\partial y} + \bar{w}^L\frac{\partial \bar{\chi}^L}{\partial z} = \bar{S}^L. \tag{9.4.14}$$

In Eq. (9.4.14) there are no flux terms corresponding to resolved eddies, since the averaging is with respect to a tube that follows the parcel motions under the influence of the waves. There is of course still a diffusive effect of unresolved eddy motions, but this must be included in the source term.

This formulation gives a finite-amplitude version of the nontransport theorem mentioned above, which states that for steady, conservative waves $\bar{v}^{\mathrm{L}} = \bar{w}^{\mathrm{L}} = 0$ and hence $\bar{\chi}_t^{\mathrm{L}} = \bar{S}^{\mathrm{L}}$; the net transport again vanishes. A physical interpretation is that under the stated conditions the orbits of resolved fluid parcels, although wavy, are "statistically closed," in the sense that no large-scale dispersion or Lagrangian-mean advection can occur. Hence the parcels can accomplish no systematic meridional transport.

Using the small-amplitude GLM theory introduced in Section 3.7.2, it can be shown that

$$\bar{v}^{\mathrm{L}} = \bar{v}^{\dagger} + \tfrac{1}{2}(\overline{\eta'^2})_{ty} + \tfrac{1}{2}\rho_0^{-1}(\rho_0\overline{\eta'\zeta'})_{tz} + O(\alpha^3), \tag{9.4.15a}$$

$$\bar{w}^{\mathrm{L}} = \bar{w}^{\dagger} + \tfrac{1}{2}(\overline{\eta'\zeta'})_{ty} + \tfrac{1}{2}\rho_0^{-1}(\rho_0\overline{\zeta'^2})_{tz} + O(\alpha^3). \tag{9.4.15b}$$

From Eqs. (9.4.15) and (9.4.9c), it is readily verified that

$$(\rho_0\bar{v}^{\mathrm{L}})_y + (\rho_0\bar{w}^{\mathrm{L}})_z = \tfrac{1}{2}(\rho_0\overline{\xi_j\xi_k})_{,jkt} = (\rho_0\mathbf{K}_{jk}^{(\mathrm{s})})_{,jk} \tag{9.4.16}$$

where indices j, k are summed over the values 2, 3 designating the meridional and vertical directions, respectively, and $\mathbf{K}^{(\mathrm{s})}$ is the "diffusion" tensor defined in Eq. (9.4.8). Thus, in the GLM system the divergence in the meridional plane does not generally vanish for transient eddies, in which air parcels are dispersing from their mean positions (see Section 3.7.1). If, however, the waves are *linear and steady*, no dispersion occurs, and the divergence vanishes.

In practice the GLM model is not very useful, since when eddy motions are strongly transient the wavy tubes quickly become highly convoluted so that the motion of the "center of mass" defined by the Lagrangian mean may bear little relation to the actual tracer distribution. For adiabatic and frictionless motion the wavy tubes along which the GLM averages are computed coincide with the intersections of θ and P surfaces, and we have already seen in Section 5.2.3 that planetary wave breaking processes lead to rapid distortion, and even "breaking" of such tubes. Only for small-amplitude eddies do these difficulties not arise.

9.4.3 The Isentropic Formulation

The isentropic coordinate approach has some of the conceptual advantages of the GLM formulation without as many of the accompanying technical difficulties. In this system the "vertical velocity" is proportional

to the diabatic heating rate, $D\theta/Dt = Q$ [see Eq. (3.1.3e)]. Thus, the tracer continuity equation [Eq. (9.4.1)] is

$$\chi_t + u\chi_x + v\chi_y + Q\chi_\theta = S. \tag{9.4.17a}$$

The Cartesian coordinate version of the continuity equation [Eq. (3.8.1c)] is

$$\sigma_t + (\sigma u)_x + (\sigma v)_y + (\sigma Q)_\theta = 0. \tag{9.4.17b}$$

where the "density" σ is defined in Eq. (3.8.1e). Multiplying Eq. (9.4.17a) by σ and Eq. (9.4.17b) by χ and adding, we obtain the flux form of the tracer continuity equation,

$$(\sigma\chi)_t + (\sigma u\chi)_x + (\sigma v\chi)_y + (\sigma Q\chi)_\theta = (\sigma S). \tag{9.4.18}$$

Averaging zonally (with θ held constant) we get from Eq. (9.4.18)

$$\bar{\sigma}\bar{\chi}_t + (\overline{\sigma v})\bar{\chi}_y + (\overline{\sigma Q})\bar{\chi}_\theta = \overline{\sigma S} - (\overline{\sigma'\chi'})_t - [\overline{(\sigma v)'\chi'}]_y - [\overline{(\sigma Q)'\chi'}]_\theta. \tag{9.4.19}$$

As in Eq. (3.9.5), we define a mass-weighted mean for any field A:

$$\bar{A}^* \equiv (\overline{\sigma A})/\bar{\sigma}.$$

Then from Eq. (9.4.17b) we obtain

$$\bar{\sigma}_t + (\bar{\sigma}\bar{v}^*)_y + (\bar{\sigma}\bar{Q}^*)_\theta = 0 \tag{9.4.20}$$

[cf. Eq. (3.9.7c)], while Eq. (9.4.19) can be expressed in the exact form

$$\bar{\chi}_t + \bar{v}^*\bar{\chi}_y + \bar{Q}^*\bar{\chi}_\theta = \bar{S}^* - \bar{\sigma}^{-1}(\overline{\sigma'\chi'})_t - \bar{\sigma}^{-1}\{[\overline{(\sigma v)'\chi'}]_y + [\overline{(\sigma Q)'\chi'}]_\theta\}. \tag{9.4.21}$$

The linearized disturbance equation is

$$\bar{D}\chi' + v'\bar{\chi}_y + Q'\bar{\chi}_\theta = S' + O(\alpha^2), \tag{9.4.22}$$

where we have assumed that $\bar{\chi}_t$, $\bar{v}$, $\bar{Q}$, $\bar{S} = O(\alpha^2)$, and α is as usual a measure of the disturbance amplitude. Here $\bar{D} \equiv \partial/\partial t + \bar{u}\,\partial/\partial x$. It should be noted that since derivatives and averages are taken at constant θ, the definitions of the "disturbance" quantities differ slightly from the z-coordinate versions discussed earlier in this section. We define perturbation quantities η', q', γ' by

$$\bar{D}(\eta', q', \gamma') = (v', Q', S') + O(\alpha^2). \tag{9.4.23}$$

From Eqs. (9.4.22) and (9.4.23) we then obtain

$$\chi' = -\eta'\bar{\chi}_y - q'\bar{\chi}_\theta + \gamma' + O(\alpha^2). \tag{9.4.24}$$

By analogy to our treatment of the conventional Eulerian-mean equation, we define

$$\mathbf{K}^{(s)} \equiv \tfrac{1}{2}\begin{bmatrix} (\overline{\eta'^2})_t & (\overline{\eta'q'})_t \\ (\overline{\eta'q'})_t & (\overline{q'^2})_t \end{bmatrix}, \tag{9.4.25a}$$

$$\Psi \equiv \tfrac{1}{2}(\overline{v'q'} - \overline{\eta'Q'}), \tag{9.4.25b}$$

$$\bar{v}^{\dagger} \equiv \bar{v}^{*} + \bar{\sigma}^{-1}(\bar{\sigma}\Psi)_{\theta}, \tag{9.4.25c}$$

$$\bar{Q}^{\dagger} \equiv \bar{Q}^{*} - \bar{\sigma}^{-1}(\bar{\sigma}\Psi)_{y} \tag{9.4.25d}$$

and obtain from Eq. (9.4.21) the isentropic coordinate form of the zonal mean tracer transport equation:

$$\bar{\chi}_t + \bar{v}^{\dagger}\bar{\chi}_y + \bar{Q}^{\dagger}\bar{\chi}_{\theta} = \bar{S}^{*} - \bar{\sigma}^{-1}(\overline{\sigma'\chi'})_t - \bar{\sigma}^{-1}[(\bar{\sigma}\overline{v'\gamma'})_y + (\bar{\sigma}\overline{Q'\gamma'})_{\theta}] + \bar{\sigma}^{-1}\nabla_{\theta}\cdot[\bar{\sigma}\mathbf{K}^{(s)}\cdot\nabla_{\theta}\bar{\chi}] + O(\alpha^3). \tag{9.4.26}$$

If the eddies are *adiabatic* ($Q' = q' = 0$), then the components $K_{y\theta}$, $K_{\theta y}$, and $K_{\theta\theta}$ all vanish, $\Psi = 0$, and $(\bar{v}^{\dagger}, \bar{Q}^{\dagger}) = (\bar{v}^{*}, \bar{Q}^{*})$; if in addition we neglect terms in σ', Eq. (9.4.26) simplifies to

$$\bar{\chi}_t + \bar{v}^{*}\bar{\chi}_y + \bar{Q}^{*}\bar{\chi}_{\theta} = \bar{S}^{\dagger} + \bar{\sigma}^{-1}\frac{\partial}{\partial y}\left[\bar{\sigma}K_{yy}\frac{\partial\bar{\chi}}{\partial y}\right], \tag{9.4.27}$$

where the diffusion coefficient $K_{yy} \equiv \frac{1}{2}(\overline{\eta'^2})_t$ is a measure of dispersion of parcels on isentropic surfaces and

$$\bar{S}^{\dagger} \equiv \bar{S}^{*} - \bar{\sigma}^{-1}(\bar{\sigma}\overline{v'\gamma'})_y \tag{9.4.28}$$

is a modified source term [cf. Eq. (9.4.9d)].

When S' can be modeled as a weak linear relaxation, manipulations analogous to those leading to Eq. (9.4.10) yield from Eq. (9.4.28)

$$\bar{S}^{\dagger} = \bar{S}^{*} - \bar{\sigma}^{-1}(\bar{\sigma}\overline{\eta'\gamma'})_{ty} + \bar{\sigma}^{-1}\frac{\partial}{\partial y}\left(\bar{\sigma}\hat{K}_{yy}\frac{\partial\bar{\chi}}{\partial y}\right) \tag{9.4.29}$$

where $\hat{K}_{yy} \equiv A\overline{\eta'^2}$. Substitution from Eq. (9.4.29) into Eq. (9.4.27) then gives

$$\bar{\chi}_t + \bar{v}^{*}\bar{\chi}_y + \bar{Q}^{*}\bar{\chi}_{\theta} = \bar{S}^{*} - \bar{\sigma}^{-1}(\bar{\sigma}\overline{\eta'\gamma'})_{ty} + \bar{\sigma}^{-1}\frac{\partial}{\partial y}\left[\bar{\sigma}K^{(\mathrm{tot})}\frac{\partial\bar{\chi}}{\partial y}\right] \tag{9.4.30}$$

where $K^{(\mathrm{tot})} \equiv K_{yy} + \hat{K}_{yy}$. If the eddies are *steady* as well as being *linear* and *adiabatic*, the second term on the right-hand side in Eq. (9.4.30) vanishes and $K^{(\mathrm{tot})}$ reduces to $\hat{K}_{yy}$.

As mentioned at the end of Section 9.3.1, the observed slopes of mixing ratio surfaces in the meridional plane for long-lived species such as N_2O and CH_4 are substantially less than would occur if the only processes operating were advection by the diabatic circulation and chemical destruction. The isentropic form of the transport equation [Eq. (9.4.30)] clearly indicates that the additional process required to explain the observations is meridional mixing by quasi-isentropic eddies. Thus, as summarized in Fig. 9.4, the gross characteristics of transport in the meridional plane can be modeled in terms of a combination of advection by a mean meridional mass circulation and quasi-isentropic mixing by large-scale eddies.

In particular, the angle between the streamlines of the circulation and the mean mixing ratio surface is related to the eddy diffusion in Eq. (9.4.27) or Eq. (9.4.30). For example, in the steady state, Eq. (9.4.20) implies the existence of a stream function, $\tilde{\Psi}$ say, such that

$$\bar{\sigma}\bar{v}^* = -\tilde{\Psi}_\theta, \qquad \bar{\sigma}\bar{Q}^* = \tilde{\Psi}_y;$$

substitution into Eq. (9.4.27) gives

$$-\tilde{\Psi}_\theta \bar{\chi}_y + \tilde{\Psi}_y \bar{\chi}_\theta = \frac{\partial}{\partial y}\left[\bar{\sigma} K_{yy} \frac{\partial \bar{\chi}}{\partial y}\right]$$

if $\bar{\chi}_t$ and $\bar{S}^\dagger$ are set to zero. The angle between the streamlines and the $\bar{\chi}$ surfaces is thus

$$\sin^{-1}\left[\frac{\dfrac{\partial}{\partial y}\left(\bar{\sigma} K_{yy} \dfrac{\partial \bar{\chi}}{\partial y}\right)}{|\nabla_\theta \tilde{\Psi}| \cdot |\nabla_\theta \bar{\chi}|}\right]$$

in $y\theta$ space: this vanishes for $K_{yy} = 0$, in which case the tracer isolines coincide with streamlines. When $K_{yy} > 0$, the tracer isolines slope less steeply than the streamlines in high latitudes, as shown schematically in Fig. 9.4.

9.5 Dispersive Wave Transport: Irreversible Mixing of Tracers

The derivation of equations like Eqs. (9.4.7) and (9.4.27), exhibiting eddy terms of "diffusive" form, has assumed the eddies to be of small amplitude. Under this assumption, diffusion coefficients like $K_{yy} = \frac{1}{2}(\eta'^2)_t$ represent *reversible* dispersion of fluid parcels: $K_{yy} > 0$ if η'^2 increases with time as parcels disperse, but $K_{yy} < 0$ as η'^2 decreases again if parcels return to their equilibrium latitudes. For finite-amplitude disturbances we can expect more complex behavior, whose representation by equations like Eqs. (9.4.7) and and (9.4.27) may be more difficult to justify rigorously. In Section 5.2.3 we discussed the dynamical implications of so-called planetary wave breaking. We there emphasized that "wave breaking" in this context refers to a rapid irreversible deformation of otherwise wavy material contours. The ability of organized quasi-nondivergent velocity fields to generate such irreversible deformation is illustrated by the classic example of Fig. 9.5, which clearly shows the tendency for flows to string a conservative tracer out into ever longer, thinner laminae, so that ultimately small-scale turbulence can mix the tracer throughout the domain. In strongly nonlinear situations of this kind, parcels certainly do not return to their original latitudes, even in statistically steady flow, and the small-amplitude theory would appear to

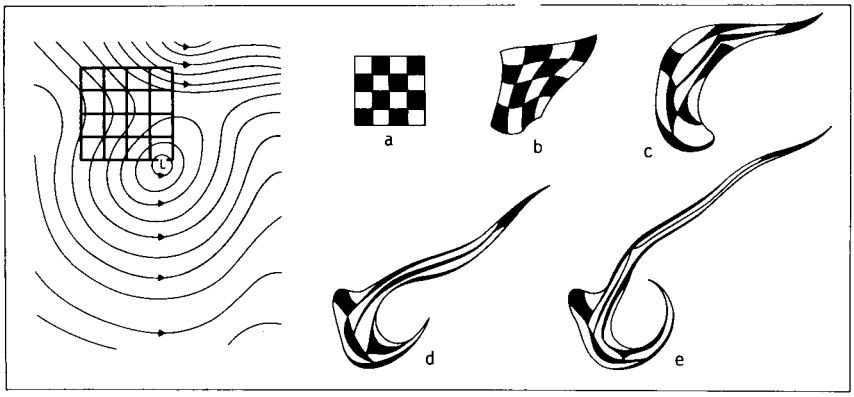

Fig. 9.5. The evolution of the shape of a set of marked fluid parcels initially forming a "checkerboard" pattern under the influence of a two-dimensional deformation field (shown on the left) typical of that occurring in large scale barotropic atmospheric eddies. For all practical purposes the deformation may be regarded as irreversible. [After Welander (1955).]

be invalid. Nevertheless, experiments with a numerical model (Plumb and Mahlman, 1987) suggest that Eqs. (9.4.7) and (9.4.27) may still describe such irreversible mixing quite well, although the components of $\mathbf{K}^{(s)}$ no longer have simple expressions in terms of parcel displacements: see Section 9.7.1.

The planetary wave breaking process, by which isentropic potential vorticity distributions are mixed in the stratospheric surf zone, will thus tend to mix chemical tracers that have meridional gradients on isentropic surfaces. For timescales that are shorter than the chemical and radiative timescales, the behavior of such chemical tracers should be very similar to that of potential vorticity, provided that the mean gradients are similar. The long-lived tracers discussed in Section 9.2 are excellent examples of such tracers, since they all, like potential vorticity, have strong vertical gradients in the lower stratosphere. Global measurements of two of these tracers, N_2O and CH_4, are available from the SAMS instrument on *Nimbus* 7. Despite the limited resolution of the observations, there is clear evidence of material line deformation during planetary wave breaking as shown in the methane maps of Figs. 9.6a,b. (These should be compared with the isentropic potential vorticity charts of Figs. 9.6c,d.)

Similar evidence is available for ozone, as measured by the LIMS experiment. Although ozone has a chemical timescale in the polar night that is much longer than the dissipation timescale for potential vorticity, it does not have a strong vertical gradient in the midstratosphere as does the potential vorticity P. Nevertheless, observations during the strong wave amplification of late January 1979 indicate that ozone and potential

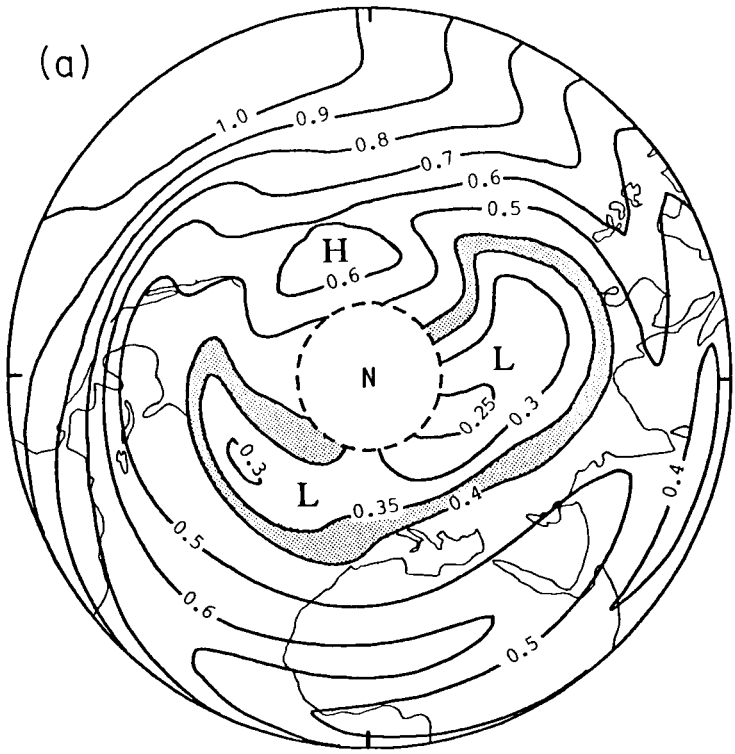

Fig. 9.6. Polar stereographic maps (Greenwich meridian at bottom) of CH_4 (ppmv) at 3 mb on (a) December 1, 1981 and (b) December 6, 1981. (Outer circle, equator; inner circle, $67\frac{1}{2}°$N.) Ertel's potential vorticity P on the 850 K isentropic surface (near 10 mb) in units of 10^{-4} K m^2 kg^{-1} s^{-1} on (c) December 1, 1981 and (d) December 6, 1981. Geostrophic winds are indicated by arrows. [After Jones (1984); (c) and (d) courtesy of A. O'Neill, U.K. Meteorological Office.] *Figure continues.*

vorticity are irreversibly mixed in similar ways (see Section 5.2.3). However, during the major stratospheric warming period of late February 1979, ozone does not follow P quite as well as during the earlier period, apparently due to the fact that the chemical time-scale for ozone in the polar night is much longer than the radiative timescale, so that the potential vorticity distribution tends to recover more rapidly following transport into the polar region than does ozone. A result of the repeated penetration of ozone-enriched tongues of air into the polar night is a gradual buildup of ozone in this region, far from the photochemical source.

In summary, the evidence from SAMS and LIMS is that rapid quasi-isentropic meridional transport is associated with planetary wave breaking events, and that this process tends to reduce the meridional gradients of

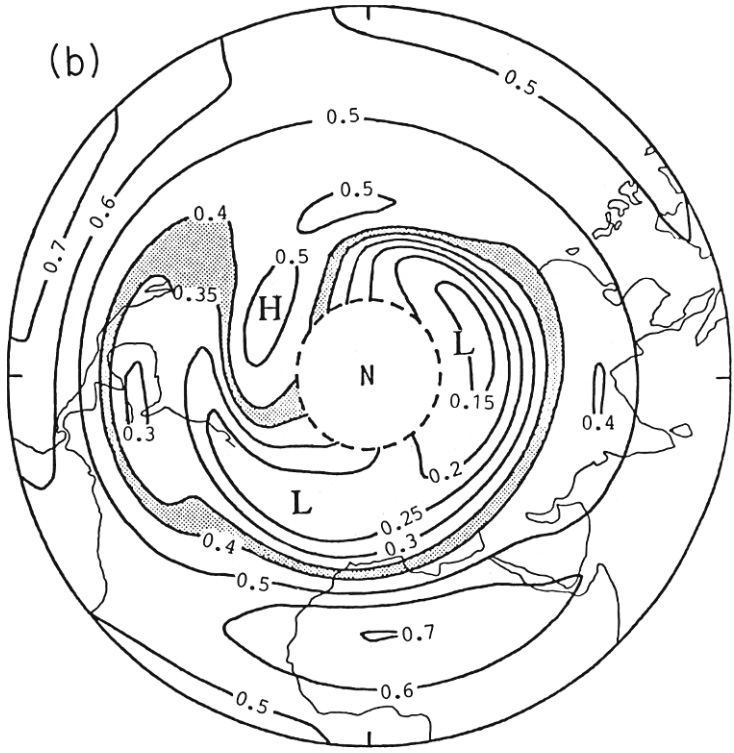

Fig. 9.6 (*figure continues*)

quasi-conserved tracers on isentropic surfaces. In particular, the ozone "hole" observed in the northern polar region during the early winter is gradually filled during the course of the winter by repeated poleward penetrations of low-latitude air parcels advected by breaking waves. Thus, large-amplitude wave motions, through nonlinear processes, produce quasi-isentropic mixing of long-lived stratified tracers, which limits the meridional gradients continually generated by the diabatic circulation.

9.5.1 Vertical Variance of Long-Lived Tracers

In the previous section we emphasized the hemispheric-wide role of planetary wave breaking, and implicitly assumed that the vertical scales of the motions were quite large, since available satellite measurements do not resolve structures with vertical scales less than a few kilometers. However, when the motion field is highly baroclinic, as is often the case in the lower stratosphere in winter, isentropic trajectories for levels separated by only a kilometer or two may differ substantially.

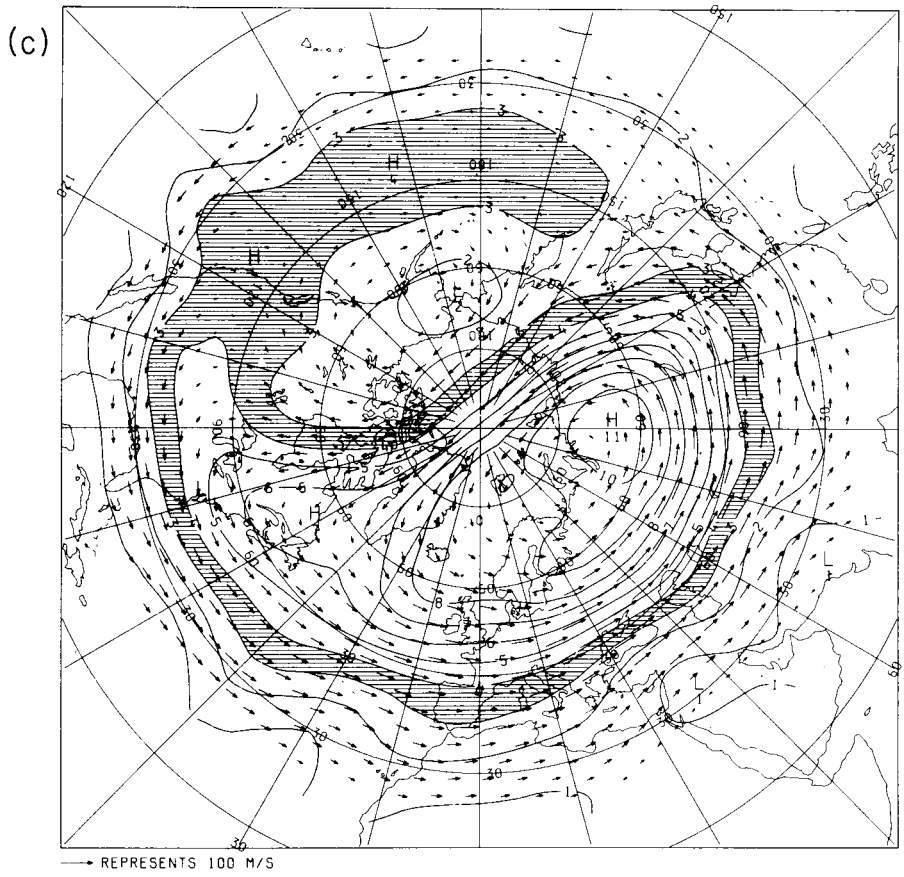

Fig. 9.6 (*figure continues*)

A spectacular example of the consequences that this has for local vertical profiles is shown in Fig. 9.7. In this sounding from Laramie, Wyoming, on January 31, 1979, both the ozone and water-vapor traces show distinct minima at the 15-km level. Minima of this type are commonly seen in ozonesonde records and have in the past generally been interpreted as arising from quasi-horizontal transport from the midlatitude upper troposphere (where ozone mixing ratios are very low) into the lower stratosphere. However, the existence of correlated water vapor and ozone minima in the sounding strongly suggests a tropical source, since water-vapor mixing ratios as low as 3 ppmv normally occur only in the lower tropical stratosphere. Furthermore, air originating in the extratropical troposphere would need to be heated diabatically by about 30 K in order to ascend to the 15-km

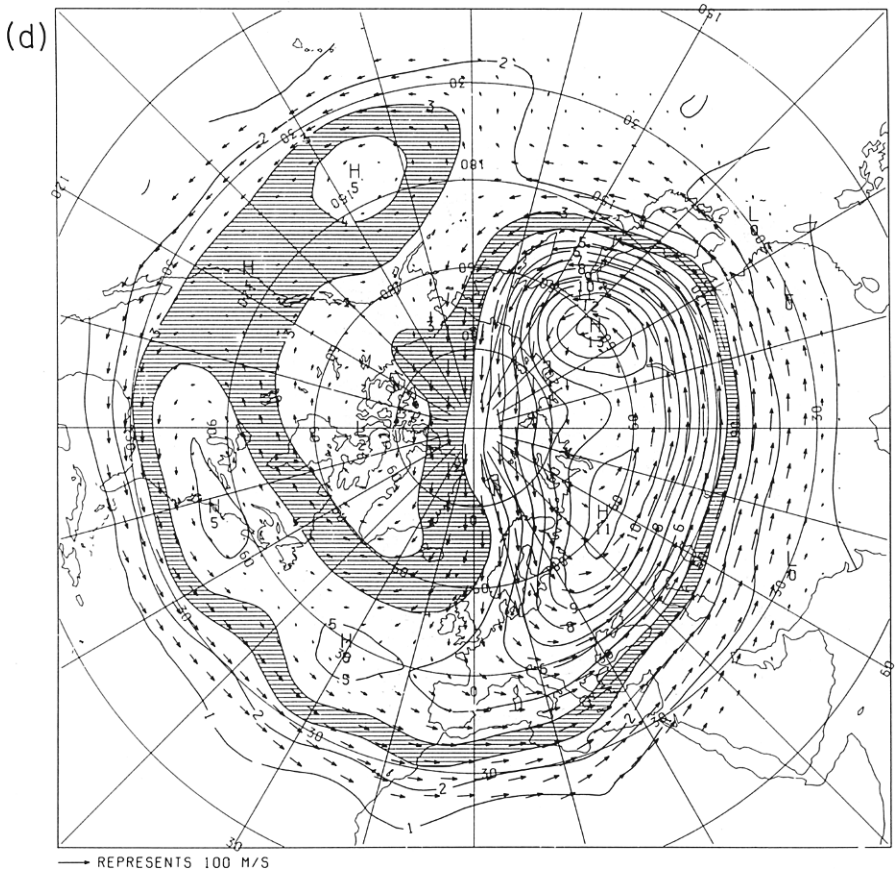

Fig. 9.6 (*continued*)

level. Such heating would be very unlikely to occur in the several-day timescale implied by the sharpness of the ozone minimum.

Danielsen and Kley (1987) constructed isentropic trajectories for several levels (marked by the potential temperature values indicated on Fig. 9.7) for a period beginning 5 days prior to the Laramie sounding. The resulting trajectories shown in Fig. 9.8 indicate that at all levels except the 406-K isentrope the air has its recent origins in the extratropical stratosphere. (Note the cross-polar trajectory at 660 K; this is caused by the amplification of the Aleutian anticyclone associated with a minor stratospheric warming.) Only at the level of the observed correlated ozone and water-vapor minima does the air have a tropical origin—in the equatorial Western Pacific. This tropical origin is consistent with the observed positive correlation between

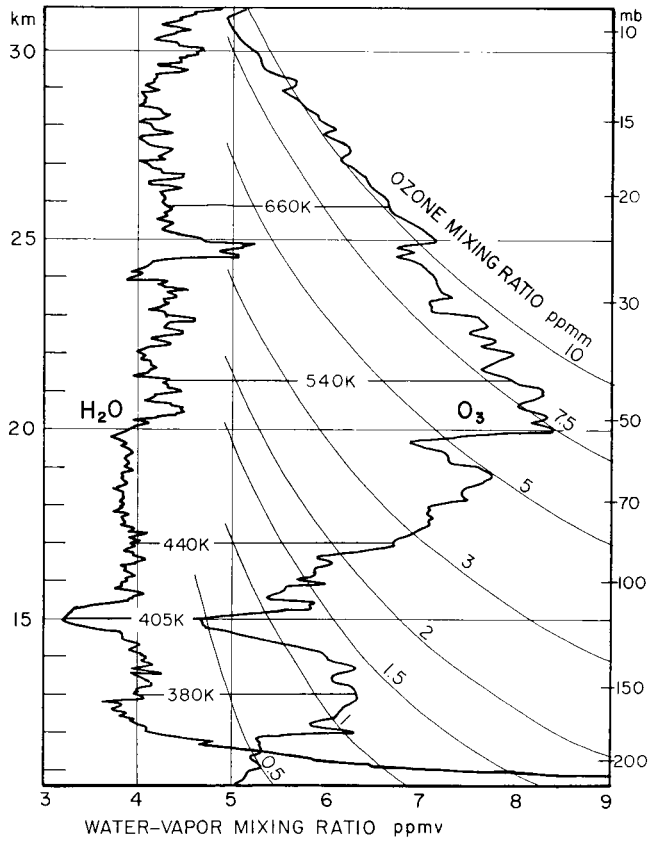

Fig. 9.7. Profiles of water-vapor and ozone mixing ratios in the stratosphere at Laramie, Wyoming, January 31, 1979. To emphasize variability at the lower altitudes the ozone plot is linear in ozone partial pressure; thus, lines of constant ozone mixing ratio are curves sloping upward toward the left. Notice the correlated ozone and water-vapor minima at the 405-K isentropic level. The isentropic levels used for the trajectory analysis in Fig. 9.8 are shown on the diagram. [After Danielsen and Kley (1987).]

the ozone and water-vapor fluctuations, since such air probably was recently "freeze dried" by passage through the cold tropical tropopause.

This example of short-vertical-scale tracer variability suggests one way in which planetary-scale wave breaking may lead to irreversible mixing. The vertical structure in the velocity field allows the fluid deformations to bring tongues of air from vastly different regions into close contact—both horizontally and vertically. Thus very strong gradients are formed, as shown

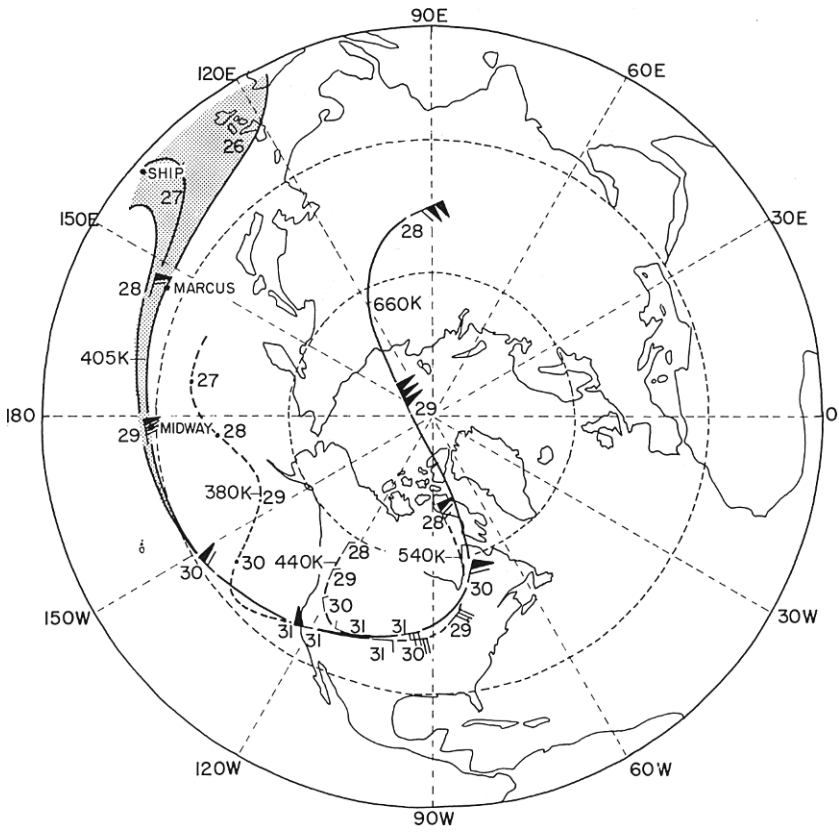

Fig. 9.8. Isentropic trajectories on $\theta = 380$, 405, 540, and 660 K surfaces for the 5-day period ending January 31, 1979. Dated wind barbs show rate of progress of an air parcel along the trajectory. [After Danielsen and Kley (1987).]

in Fig. 9.7. These gradients will inevitably be smoothed by small-scale diffusion so that mid- and low-latitude properties become mixed. Of course, vertical diffusion is generally slow in the stratosphere where the static stability is very large, but even an eddy diffusivity as small as $0.25\ m^2\ s^{-1}$ will mix the short-vertical-scale structure of this example in less than 10 days.

9.5.2 Temporal Variance of Stratospheric Trace Species

For the long-lived vertically stratified tracers discussed in Section 9.2, oscillatory vertical motions can produce temporal variance at a given point in physical space merely through vertical displacements of the isentropes.

However, as suggested in Fig. 9.4, such tracers tend to have meridional gradients on isentropic surfaces. Hence, simple meridional sloshing of zonally propagating adiabatic wave motions can produce temporal variance in tracer profiles at a single location; vertical displacements of the isentropes are not required. This phenomenon does not depend on nonlinear wave processes such as planetary wave breaking; nor does it necessarily imply mixing or irreversibility.

Observed temporal variability is conveniently characterized by an "equivalent displacement height" (EDH) (Ehhalt *et al.*, 1983). The EDH is the vertical distance that the time-mean vertical tracer profile would need to be displaced in order to produce the locally observed variance. The use of the EDH to characterize tracer variability should not be taken to imply that it is primarily vertical displacements that act to product the variance. Meridional displacements may actually be more important. The relative roles of meridional and vertical parcel displacements can be assessed approximately by comparing the EDH for potential temperature with that for long-lived chemical tracers, since the meridional tracer slopes are generally greater than the slopes of the isentropes (see Section 9.2).

For conservative waves the linear tracer perturbation equation [Eq. (9.4.6)] for departures from zonal symmetry is

$$\chi' = -\eta'\bar{\chi}_y - \zeta'\bar{\chi}_z. \tag{9.5.1}$$

If it is assumed that the temporal variation at a local point is similar to the spatial variation around a latitude circle, then the EDH can be defined as $\delta_\chi \equiv (\overline{\chi'^2})^{1/2}/\bar{\chi}_z$. Thus using Eq. (9.5.1),

$$\delta_\chi = \overline{[(\eta'[\bar{\chi}_y/\bar{\chi}_z] + \zeta')^2]}^{1/2}, \tag{9.5.2}$$

which shows that the EDH is just the eddy displacement normal to the mean slope of the tracer isopleths. For species with long chemical timescales, the mean tracer slopes in the meridional plane, $[dz/dy]_{\bar{\chi}} = -\bar{\chi}_y/\bar{\chi}_z$ are generally large enough so that the contribution to δ_χ by η' is at least as large as that due to ζ'. For planetary wave breaking, it is indeed quasi-horizontal displacements that play the major role in producing tracer variance.

The altitude dependence of the magnitudes of the EDHs for a number of species measured in Northern Europe in summer are summarized in Fig. 9.9. Measurements of temperature show that the EDH for potential temperature at a given height is an order of magnitude smaller than the EDHs for the trace chemicals. This indicates that the observed variance is not the result of vertical displacement of the isentropic surfaces, as would be produced by internal gravity waves, for example. The variance might,

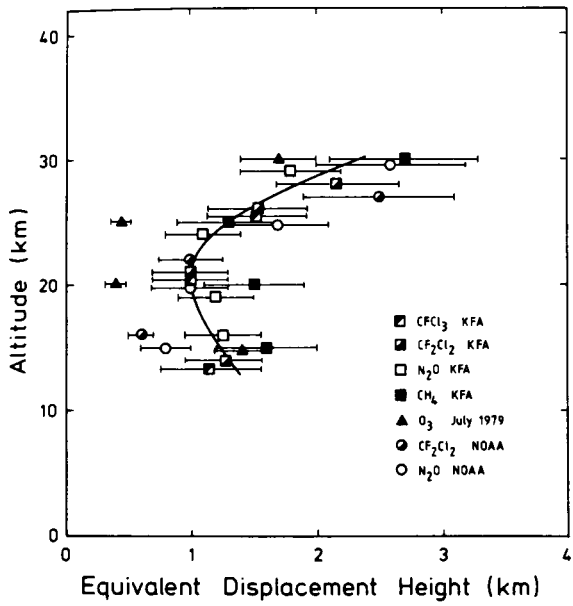

Fig. 9.9. Magnitudes of equivalent displacement heights (EDH) for several long-lived trace gases. See text for definition and significance. [From Ehhalt *et al.* (1983), with permission.]

however, be associated with meridional displacements produced by quasi-barotropic wave motions such as the 5-day wave (see Section 4.4). For observed tracer isopleth slopes, an EDH of 2 km could be produced by meridional displacement of about 1000 km.

It is conceivable, however, that some of the tracer variability observed in the middle stratosphere during the summer is not associated with active wave motions, but represents variance generated by the large meridional and vertical parcel displacements associated with the springtime final warming process that has become "frozen in" and is merely advected around by the symmetric easterly circulation of the summer stratosphere. Such a situation might arise for any tracer whose dissipation timescale is substantially longer than the dynamical timescale. For the final warming, which is marked by breakdown of the winter polar vortex and establishment of the summer polar circulation, the relevant dynamical timescale is the scale on which radiation damps out the wave motions. This scale is of the order of 1–3 weeks in the stratosphere (depending on height) and is substantially shorter than the chemical decay times for the long-lived species considered here. Thus, tongues of air with either enriched or depleted tracer concentrations might possibly persist for a very long time in the summer stratosphere, where diffusion should be quite weak.

9.6 Troposphere–Stratosphere Exchange

Transport of trace substances is important to understanding of tracer behavior in both the troposphere and the stratosphere. Especially important, however, is the vertical flux of trace constituents across the tropopause and through the lowest few kilometers of the stratosphere. It is this region that primarily determines the rate of transport between source and sink regions for both tropospheric and stratospheric source gases. For example, the slowness of transport in this region is responsible for the observed long stratospheric residence times for radioactive tracers, and for the long time needed to establish a steady-state ozone reduction in response to tropospheric release of chlorofluoromethanes (see Section 10.5.3). Thus, the dynamics of exchange across the tropopause merits special consideration. Other aspects of troposphere-stratosphere linkage are considered in Chapter 12.

Conventionally, the tropopause is defined on the basis of the thermal structure of the atmosphere as the level of near discontinuity in the temperature lapse rate that divides the strongly statically stable stratosphere from the weakly statically stable troposphere (Figs. 1.1 and 9.1a). For climatological purposes this definition may be satisfactory. However, lapse rate is not a conservative quantity, and for discussion of exchange of mass between the troposphere and the stratosphere it is preferable to use Reed's (1955) concept of a dynamical tropopause defined in terms of the near discontinuity in Ertel's potential vorticity that separates very large stratospheric values from tropospheric values that are one or two orders of magnitude smaller (see Fig. 9.1b). Thus "exchange" requires that air parcels of stratospheric (tropospheric) origin lose (gain) potential vorticity through mixing or diabatic processes, and the rate of exchange is controlled by the rate at which such processes operate.

Transport across the tropopause may be caused by a number of processes. These include (1) the large-scale mean diabatic circulation (Brewer–Dobson cell), (2) transverse secondary circulations associated with subtropical and polar jetstreams, (3) cumulonimbus clouds penetrating into the stratosphere, (4) tropopause folding and subsequent mixing caused by upper-level cyclogenesis, (5) turbulent mixing associated with gravity-wave breaking or with shear instabilities at the tropopause, and (6) local radiative cooling in the vicinity of high-level cirrus anvil clouds.

Cross tropopause exchange in middle latitudes is dominated by tropopause folding associated with the development of upper-level baroclinic waves in the tropospheric jetstream. The term "folding" is used to describe a process in which the dynamical tropopause (defined in terms of potential vorticity) intrudes deeply into the troposphere along a sloping

frontal zone (see Fig. 9.10). Studies of both chemical and dynamical tracers during such folding events have done much to elucidate the nature of this process, which is perhaps the primary mechanism for transport of mass from the stratosphere into the troposphere. The return flow from troposphere to stratosphere appears to take place primarily in the equatorial region, as suggested by the Brewer–Dobson model discussed above. However, the actual mechanism appears to involve cumulus convection rather than gentle large-scale ascent.

9.6.1 Extratropical Exchange: Tropopause Folding

The tropopause folding process has its origins in the deformation field associated with upper-level frontogenesis occurring as a result of baroclinic instability in the westerly jetstreams. According to the accepted theory of frontogenesis (Hoskins, 1982), the geostrophic deformation field associated with the development of a baroclinic wave tends to concentrate preexisting temperature gradients, thus giving rise to a sloping zone of closely spaced isentropes that marks the boundary between cold and warm air masses. This concentration is most intense near the ground and the tropopause. To

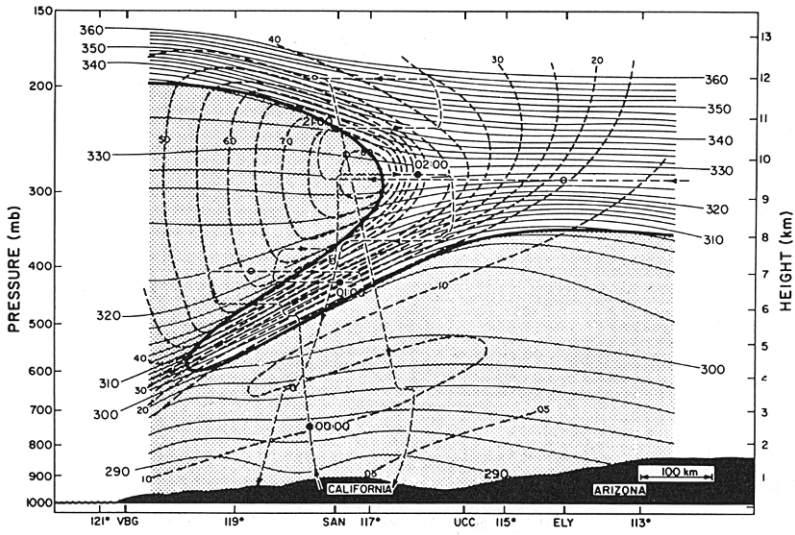

Fig. 9.10. Cross section through tropopause folding event of March 13, 1978: region of tropospheric air stippled; potential temperature (thin solid lines); wind speed ($m\,s^{-1}$, dashed lines); research aircraft flight track (thin dashed lines); potential vorticity tropopause (heavy solid line). [From Shapiro (1980). American Meteorological Society.]

maintain the thermal wind balance under such conditions, a secondary transverse ageostrophic circulation arises. Advection by this secondary circulation further concentrates the temperature gradient, which enhances the secondary circulation, and so on. This process leads to a rapid intensification of the temperature gradient and at the same time forces strong parcel subsidence in the frontal zone. This subsidence advects high potential vorticity air parcels of stratospheric origin downward along the sloping isentropic surfaces, so that the dynamical tropopause is folded to form a deep intrusion of stratospheric air into the troposphere.

The development of such an intrusion is shown for a theoretical two-dimensional model in Fig. 9.11. Small arrows in the figure, showing fluid-parcel paths associated with the transverse ageostrophic motion, clearly indicate downward parcel motion along the frontal zone. In tropopause fold cases observed in the atmosphere, the stratospheric intrusions can be much deeper than suggested by the model of Fig. 9.11. The stratospheric air can penetrate deeply into the troposphere in thin laminae of the order of 100 km lateral scale and 1 km vertical scale. The high potential vorticities that exist in the upper portions of such folds are gradually modified by irreversible small-scale mixing with tropospheric air along the boundaries

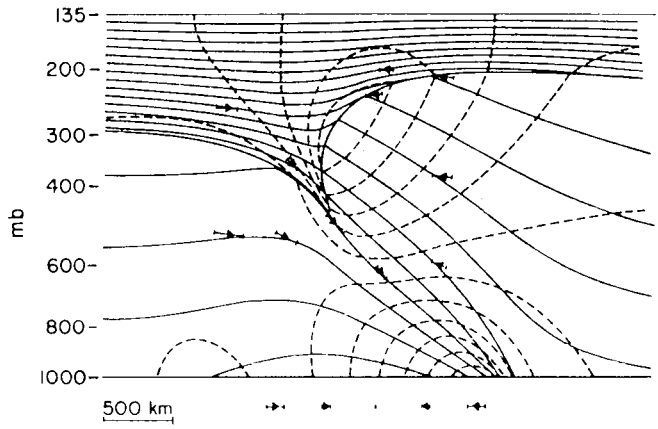

Fig. 9.11. Stratospheric intrusion generated in a model of upper-level frontogenesis caused by an applied deformation field (shown by arrows below lower surface). The initial state had a weak uniform meridional temperature gradient (warm air on right) and constant (but different) static stabilities in the troposphere and the stratosphere. Dashed contours show long front velocity (10.5 m s^{-1} interval), thin solid contours are potential temperature (7.8-K interval), and arrows within fluid show some parcel trajectories. The tropopause marks the discontinuity between widely spaced isentropes in the troposphere and closely spaced isentropes in the stratosphere. [After Hoskins (1972).]

of the fold, so that potential vorticity values and ozone mixing ratios tend to decrease moving downward along the isentropes in the folds.

This point is illustrated by the cross section in Fig. 9.12, which shows ozone mixing-ratio contours for the tropopause folding event depicted in Fig. 9.10. Figure 9.12 indicates that the fold does indeed contain air with stratospheric concentrations of ozone, but that there is substantial mixing with tropospheric air since the ozone mixing ratio decreases downward in the fold. Although Ertel's potential vorticity is not plotted, it can be deduced from the large static stability ($\partial\theta/\partial z$) and large shear vorticity present in the fold region, as depicted in Fig. 9.10, that the potential vorticity must be large in the fold.

It should be noted that in addition to the intrusion process that brings stratospheric air into the troposphere, the transverse mass circulation associated with jetstreams also transports some tropospheric air into the lower stratosphere, particularly on the anticyclonic shear (equatorward) side of the jet. Since such air must have rather high water-vapor mixing ratios, and the observed mixing ratios are very low in the stratosphere, it is believed that such return flow only transfers tropospheric air into the lowest stratospheric layers, where it may be quickly returned to the troposphere through

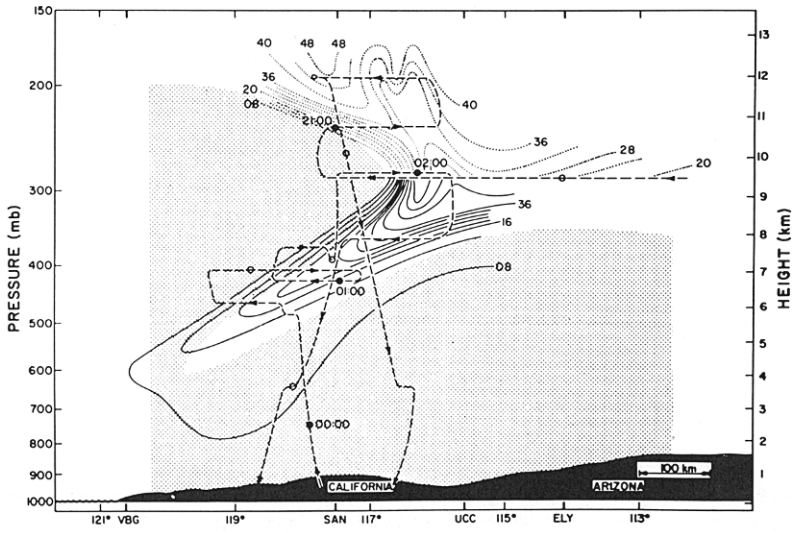

Fig. 9.12. Ozone concentration in parts per hundred million by volume for tropopause folding event shown in Fig. 9.10. Upper-flight track analysis shown in dotted lines, lower-flight track in solid lines. Stippled region indicates the troposphere. Note: warm air is on the left side, opposite to the plotting convention used in Fig. 9.11. [From Shapiro (1980). American Meteorological Society.]

the tropopause folding process. Although precise estimates are difficult, it is thought that nearly 10% of the stratospheric mass is injected into the troposphere by the folding process each year, but that most of this mass originates in the lowest part of the stratosphere.

9.6.2 Tropical Exchange: The Role of Cumulus Convection

The Brewer-Dobson model suggests that upward transfer from the troposphere into the stratosphere occurs only in the tropics, and that the rate of mass transfer is related to the diabatic heating rate. There can be little doubt that freeze drying due to upward passage of air parcels through the tropical cold trap is a qualitatively reasonable explanation for the observed extreme aridity of the stratosphere. It is certainly in general accord with the zonal mean water vapor distribution as deduced from the LIMS experiment. The LIMS water-vapor cross section shown in Fig. 9.13 clearly

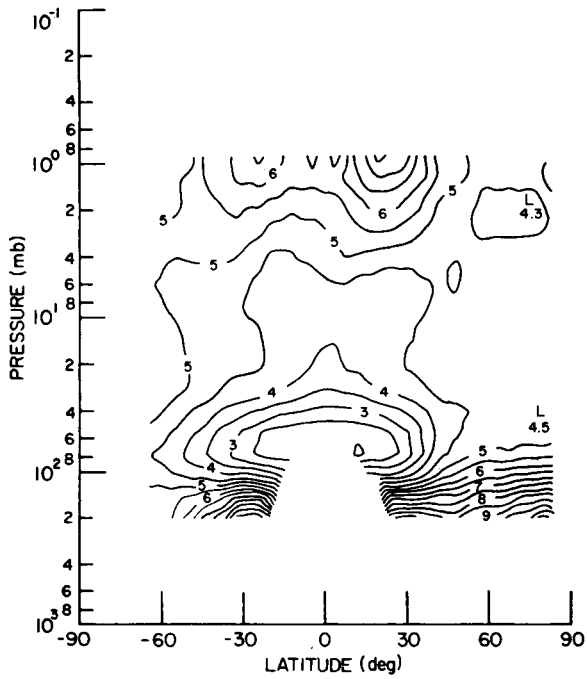

Fig. 9.13. Zonal mean water-vapor mixing ratio cross section (ppmv) for December 1978, from the *Nimbus* 7 LIMS experiment. [From Remsberg *et al.* (1984b). American Meteorological Society.]

indicates a minimum in the lower tropical stratosphere, with larger values in the upper stratosphere and at high latitudes in the lower stratosphere. This is consistent with a model in which the diabatic circulation advects a "plume" of dry air upward and poleward in both hemispheres, thus maintaining a low mixing ratio despite the presence of an upper-stratospheric source of water vapor due to methane oxidation.

Evidence from LIMS and *in situ* sampling indicates that the mean mixing ratio for water vapor in the lower stratosphere is about 3–4 ppmv. Climatological data suggest, however, that only in rather restricted regions of the tropics are the temperatures at the tropical tropopause sufficiently cold to allow freeze drying of upward-moving air to mixing ratios of less than 4 ppmv. Furthermore, observations in the Panama Canal Zone (Fig. 9.14) indicate that in that location the water-vapor minimum occurs not at the tropopause but several kilometers higher, and is also significantly smaller than the saturation mixing ratio at the tropopause level. Thus, it appears that the water-vapor distribution of the stratosphere cannot be accounted for by a model in which tropospheric air is transferred into the stratosphere locally through the slow mean motions of the diabatic circulation. Only horizontal transport from a region where the tropopause is colder and higher can plausibly account for the observed water-vapor minimum at 19 km over Panama.

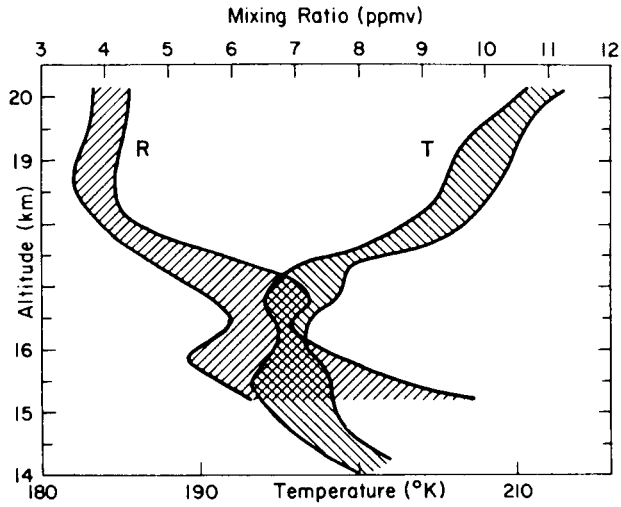

Fig. 9.14. The range of temperature (T) and water-vapor mixing ratio (R) observations for eight flights during the NASA Panama Experiment in September 1980. Areas enclosed by the diagonal lines show plus and minus 1 standard deviation from the mean. [After Kley *et al.* (1982).]

Newell and Gould-Stewart (1981) suggested that observations are consistent with a model, which they called the "stratospheric fountain," in which most of the flux of mass from the troposphere into the stratosphere is concentrated in relatively limited regions of the tropics—primarily the so-called "maritime continent" of Indonesia during the Northern-Hemisphere winter, and the Indian monsoon region during Northern-Hemisphere summer. The tropical tropopause is on the average highest and coldest at those locations and times.

It is known that much of the upward mass flux in the tropical troposphere is concentrated in the updrafts of individual cumulonimbus convective clouds. These so-called "hot towers" tend to overshoot their levels of neutral buoyancy and penetrate into the lower stratosphere, where they may mix with stratospheric air. Thus, it is likely that exchange in the tropics is associated with the convective motion scale rather than a slow uniform ascent as envisioned in the usual model for the Brewer-Dobson cell. However, the precise mechanisms of tropical exchange remain to be elucidated.

9.7 Transport Modeling

The major motivation for the development of tracer transport models in recent years has been the problem of the photochemistry of the ozone layer. Detailed analyses of this problem often involve over 100 reactions, including several dozens of chemical species. Since nearly all such species are directly or indirectly influenced by transport in the meridional and vertical directions, proper representation of transport processes is a crucial aspect of ozone-layer modeling.

Enormous computational resources would be required to compute the time-dependent ozone distribution in three dimensions. Although some progress has been made in modeling certain aspects of long-lived tracer transport in three dimensions using stratospheric general circulation models (see Chapter 11), most photochemical modeling of the ozone layer to date has been limited to either two-dimensional (latitude-height) models that average all variables in longitude or one-dimensional models that implicitly average all variables in both longitude and latitude.

The two-dimensional modeling approach is attractive for photochemical modeling because the vertical and meridional variations in species concentrations and photochemical reaction rates generally far exceed longitudinal variations. As emphasized in Section 9.3, the distribution of species in the meridional plane is not in itself determined solely by mean advection.

In two-dimensional models it is necessary to parameterize the chemical and dynamical effects of eddy motions in terms of the mean fields.

In the past, most photochemical models have been one-dimensional models in which only the global average tracer concentration can be predicted at each height. The "transport" in such models is represented entirely by vertical eddy diffusion. A rational basis for determining such one-dimensional diffusion coefficients is given in Section 9.7.3. It is first advantageous, however, to analyze the formulation of two-dimensional models.

9.7.1 Two-Dimensional Models

In Section 9.4 we discussed the formulation of two-dimensional models for tracer transport. Such models can, for example, be based on either the traditional Eulerian mean formulation, the TEM formulation, or an isentropic coordinate formulation. In each case there are certain eddy flux terms that must be parameterized and the mean flow must be specified or computed.

A few of the two-dimensional models in current use include the full set of dynamics equations in zonally averaged form. In these models the mean meridional circulation field (either the traditional Eulerian or the TEM version) is calculated from the dynamical equations for use in the tracer continuity equation. In such cases it is necessary to parameterize the eddy heat and momentum (or potential vorticity) fluxes in addition to the eddy tracer flux. Only if these fluxes are accurately represented can the mean zonal flow and mean meridional wind fields be expected to approximate reality. A simpler approach, which has been used in most two-dimensional photochemical models, is simply to externally specify the mean meridional circulation.

The earliest two-dimensional stratospheric transport models were based on the Reed and German (1965) eddy-flux parameterization, which essentially followed the Prandtl mixing-length hypothesis used in small-scale turbulence modeling. In this model it is assumed that

$$-\rho_0 \overline{\mathbf{u}'\chi'} = \mathbf{K}^{(r)} \cdot \nabla \bar{\chi},$$

where

$$\mathbf{K}^{(r)} \equiv \begin{bmatrix} K_{yy}^{(r)} & K_{yz}^{(r)} \\ K_{yz}^{(r)} & K_{zz}^{(r)} \end{bmatrix}.$$

Thus the entire effect of the eddies is incorporated in the symmetric diffusion tensor $\mathbf{K}^{(r)}$. From Eq. (9.4.3), this leads to an Eulerian mean transport equation of the form

$$\bar{\chi}_t + \bar{v}\bar{\chi}_y + \bar{w}\bar{\chi}_z = \bar{S} + \rho_0^{-1} \nabla \cdot (\rho_0 \mathbf{K}^{(r)} \cdot \nabla \bar{\chi}), \tag{9.7.1}$$

and the elements of the symmetric diffusion tensor $\mathbf{K}^{(r)}$ are empirically determined to fit observed tracer distributions.

The symmetric tensor $\mathbf{K}^{(r)}$ can be diagonalized by a coordinate transformation to principal axes orientated at an angle ε to the yz axes given by

$$\varepsilon = \frac{1}{2}\tan^{-1}\left[\frac{K_{yz}^{(r)}}{\frac{1}{2}(K_{yy}^{(r)} - K_{zz}^{(r)})}\right] \simeq \tan^{-1}\left[\frac{K_{yz}^{(r)}}{K_{yy}^{(r)}}\right], \tag{9.7.2}$$

where in the last expression we have assumed that $K_{zz}^{(r)} \ll K_{yy}^{(r)}$ and $K_{yz}^{(r)} \ll K_{yy}^{(r)}$. The symmetric tensor thus represents diffusion primarily along a sloping "mixing surface" at an angle ε to the y axis.

The Reed and German model of Eq. (9.7.1) neglects the eddy-flux contribution to the advection. This contribution, represented by the stream function Ψ defined in Eq. (9.4.9b), may be thought of as the antisymmetric component of an eddy "diffusion" tensor,

$$\mathbf{K} \equiv \mathbf{K}^{(s)} + \begin{bmatrix} 0 & \Psi \\ -\Psi & 0 \end{bmatrix}. \tag{9.7.3}$$

In terms of $\mathbf{K}$ the "effective transport velocity" formulation of Eq. (9.4.7) can be rewritten as

$$\bar{\chi}_t + \bar{v}\bar{\chi}_y + \bar{w}\bar{\chi}_z = \bar{S}^{\dagger} + \rho_0^{-1}\nabla \cdot (\rho_0 \mathbf{K} \cdot \nabla \bar{\chi}); \tag{9.7.4}$$

comparing Eq. (9.7.1) with Eq. (9.7.4), we see that a conventional two-dimensional Eulerian model should have an *asymmetric* diffusion tensor and an eddy-modified source if the mean meridional velocity is taken to be the observed Eulerian velocity $(\bar{v}, \bar{w})$. In models based on the Reed and German (1965) theory, only the symmetric components of the diffusion tensor are included; it is then necessary to empirically specify the distribution of K_{yz} to be large and negative (in the Northern Hemisphere) so that the angle ε in Eqs. (9.7.2) slopes downward steeply toward the pole. This is not surprising, since in such a model the "diffusion" must represent both the dispersive and advective effects of the wave fluxes.

In principle it would be possible to use the "correct" form of the effective transport formulation [Eq. (9.4.7)], which includes the advective effects of the eddies and the portion of the diffusion that depends on the photochemical damping rate. However, $\mathbf{K}^{(s)}$ and Ψ, which involve parcel displacements, are difficult to estimate from observed data, although as mentioned in Section 9.5, Plumb and Mahlman (1987) calculated them for the lower and middle stratosphere from a three-dimensional model. Instead, most recent Eulerian-mean models have tended to use the TEM formulation [Eq. (9.4.13)] with the residual mean $(\bar{v}^*, \bar{w}^*)$ approximated by the diabatic circulation, and a diffusion tensor on the right-hand side that is again

determined empirically. With this type of formulation it is not necessary to specify a large K_{yz} component of the diffusion tensor, since the poleward-downward transport is provided by the advection due to the diabatic circulation.

9.7.2 Isentropic Two-Dimensional Models

The isentropic coordinate approach discussed in Section 9.4.7 has both conceptual and practical advantages. Since the large-scale motions that are the dominant eddies in the stratosphere are quasi-adiabatic, reasonable accuracy in modeling stratospheric tracer distributions is possible using the simplified version of the zonally averaged isentropic transport equation, Eq. (9.4.30). The main assumption is that the "eddy diffusion" formalism in Eq. (9.4.30) can still be used to represent the irreversible mixing of tracers by large-amplitude eddies. It was mentioned in Section 9.5 that three-dimensional model experiments have given some justification for this. In such a case the relations $K_{yy} = \frac{1}{2}(\overline{\eta'^2})_t$ and $\hat{K}_{yy} = A\overline{\eta'^2}$ can no longer be expected to hold, and $K^{(\mathrm{tot})}$ has to be determined empirically or with a numerical model. Its value depends on the chemical relaxation rate, and hence separate $K^{(\mathrm{tot})}$ distributions should be used for each tracer diffused. However, including this dependence and the time-differentiated source-term modification in Eq. (9.4.30) does not seem to be essential to modeling the overall global distribution of long-lived tracers.

The other main component of the model is the advection by the isentropic-coordinate residual circulation ($\bar{v}^*$, $\bar{Q}^*$). For adiabatic eddies, $Q' = 0$ and $\bar{Q}^*$ reduces to $\bar{Q}$ [see Eq. (3.9.5)], which can be calculated from *observed* temperatures. The resulting residual circulation is thus essentially the observed diabatic circulation (see Sections 7.2 and 9.3.1). It should be noted that since the diabatic or residual circulation is primarily eddy-driven (see Chapter 7), it should not, in principle, be specified independently of the eddy diffusion coefficient K_{yy}.

A simple model for the stream function of the diabatic circulation for both solstice and equinox conditions is shown in Fig. 9.15. The diabatic circulation is dominated below 25 km by a two-cell pattern, with rising in the equatorial region, poleward motion in both hemispheres and sinking at extratropical latitudes. Above 30 km at the solstices the diabatic circulation is dominated by a single cell, with rising in the summer hemisphere, a cross-equatorial drift, and sinking in the winter hemisphere (cf. the schematic diagram of Fig. 7.2). Clearly, in the annual mean the overall pattern should resemble the equinoctial distribution of Fig. 9.15, and the mean tracer isolines for a tracer in equilibrium with the time-mean diabatic

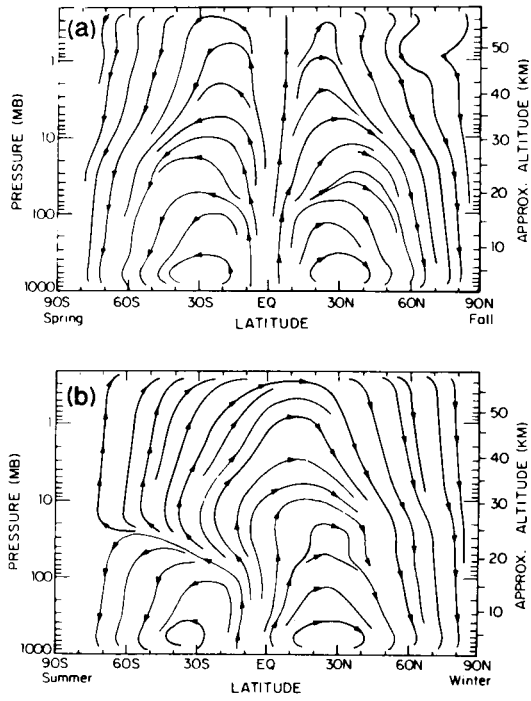

Fig. 9.15. Streamlines of a theoretical estimate of the diabatic circulation for (a) equinox and (b) solstice. [After Ko *et al.* (1985).]

circulation should thus slope downward toward the poles much more steeply than is observed for long-lived tracers such as N_2O and CH_4 (see Fig. 9.3). This suggests, as has been stressed earlier, that quasi-isentropic transport by eddies is essential to the modeling of observed tracer distributions.

The isentropic form of the two-dimensional transport equation [Eq. (9.4.27)] clearly exhibits the balance among the three key processes that determine the distribution of tracers relative to the isentropes in the meridional plane: advection by the diabatic circulation, isentropic transport by large-scale eddies, and chemical source and sinks.

Once the diabatic circulation is specified, it is still necessary, of course, to determine suitable values for K_{yy}. As noted above, the diffusion rate should in principle be related to the diabatic circulation; in particular it should depend on latitude, height, and season. However, Ko *et al.* (1985) have found that surprisingly good simulations of the N_2O distribution can be obtained by employing a constant value of $K_{yy} = 1 \times 10^5\ m^2\ s^{-1}$. The equinox and solstice distributions shown in Fig. 9.16 are in general accord with the observations shown in Fig. 9.3b. Such a model, of course, does

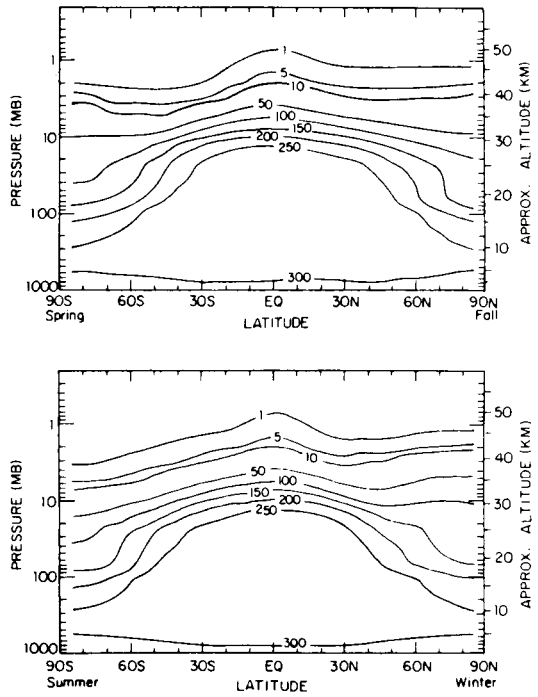

Fig. 9.16. Latitude-height distribution of N_2O mixing ratio in ppbv computed with a two-dimensional model using the diabatic circulation of Fig. 9.15 and a horizontal diffusion coefficient of $K_{yy} = 10^5\ m^2\ s^{-1}$. [After Ko *et al.* (1985).]

not reproduce all of the seasonal structure shown in the observations, and clearly should not be expected to do so since the strong mixing of the "surf zone" is not represented.

A minor disadvantage of isentropic coordinates is that the isentropes move up and down in physical space as temperatures fluctuate (e.g., with the annual cycle). Thus, the distribution of a trace species with respect to latitude and physical height may vary in time even if it remains steady in isentropic space.

9.7.3 One-Dimensional Transport Modeling

One-dimensional models that treat a vertical column of the atmosphere have been the most popular type of model for simulating photochemical cycles in the middle atmosphere. Such models by necessity can only represent transport processes in a very crude form. Formally, a one-dimensional

model can be obtained by taking a global average in the horizontal coordinates:

$$\langle \cdots \rangle = \frac{1}{4\pi} \int_0^{2\pi} \int_{-\pi/2}^{\pi/2} (\cdots) \cos\phi \, d\phi \, d\lambda.$$

When this global averaging operation is applied to the spherical coordinate version of Eq. (9.4.18), so that the averaging is done on an isentropic surface, the resulting equation has the form

$$\frac{\partial}{\partial t}\langle \sigma\chi \rangle + \frac{\partial}{\partial \theta}\langle \sigma Q\chi \rangle = \langle \sigma S \rangle. \tag{9.7.5}$$

If the diabatic heating rate is then approximated by the zonal mean, $\bar{Q}^*$, we obtain

$$\frac{\partial}{\partial t}\langle \chi \rangle + \frac{1}{\sigma_0}\frac{\partial}{\partial \theta}\langle \sigma_0 \bar{Q}^* \bar{\chi} \rangle = \langle S \rangle, \tag{9.7.6}$$

where we have also let $\bar{\sigma} = \sigma_0(\theta)$ (i.e., we define a global standard "density" that depends only on the vertical coordinate). We assume that there is an approximate balance among the last three terms in Eq. (9.4.27), and that the diffusion and chemical sinks can be parameterized in terms of linear damping at rates of τ_d^{-1} and τ_c^{-1}, respectively. Then we have

$$\bar{Q}^* \, \partial\langle \chi \rangle / \partial\theta \simeq -\bar{\chi}(\tau_d^{-1} + \tau_c^{-1}), \tag{9.7.7}$$

where we have also assumed that $\bar{\chi} \approx \langle \chi \rangle$ in the vertical advection term. Solving Eq. (9.7.7) for $\bar{\chi}$, and substituting into Eq. (9.7.6) to eliminate $\bar{\chi}$ in the vertical flux term, yields

$$\frac{\partial}{\partial t}\langle \chi \rangle - \frac{1}{\sigma_0}\frac{\partial}{\partial \theta}\left[\sigma_0 \hat{K}_{zz} \frac{\partial \langle \chi \rangle}{\partial \theta} \right] = \langle S \rangle, \tag{9.7.8}$$

where

$$\hat{K}_{zz} \equiv \langle (\bar{Q}^*)^2 (\tau_d^{-1} + \tau_c^{-1})^{-1} \rangle. \tag{9.7.9}$$

Usually $\hat{K}_{zz}$ has been empirically determined to fit observed tracer profiles. But Eq. (9.7.9) shows that if $\bar{Q}^*$ is known and τ_d and τ_c can be determined, then the vertical transport coefficient is known. Unlike most proposed one-dimensional eddy-diffusion parameterizations, the form derived here explicitly incorporates the dependence of transport on the chemical timescale for the individual tracer. Tracers with short stratospheric lifetimes

have smaller $\hat{K}$ values than do those with longer lifetimes. Some specific examples are given in Fig. 9.17.

9.7.4 *Mechanistic Three-Dimensional Transport Modeling*

In discussions of three dimensional models it is useful to distinguish between complete general circulation models (GCMs) and so-called "mechanistic" models. The former attempt to simulate the complete large-scale circulation, and they feature rather detailed representations of the various physical processes that drive the flow. The latter attempt to focus on certain aspects of the circulation by deliberately simplifying the dynamical or physical formulation. For example, some mechanistic models of the middle atmosphere do not attempt to include self-consistent calculations of the tropospheric circulation, but merely impose a specified geopotential height variation at a level near the tropopause. Other mechanistic models simplify the radiative heating and cooling by using a Newtonian cooling formulation. Dynamical simplifications may include use of the quasi-geostrophic formulation, or severely truncating the zonal wave-number spec-

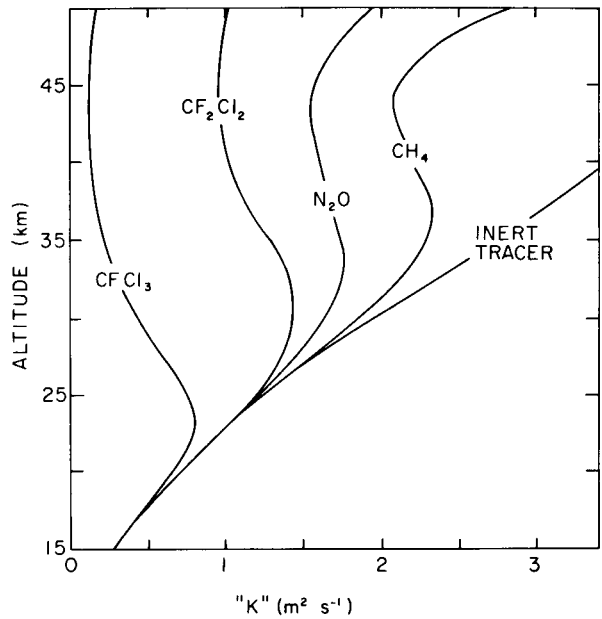

Fig. 9.17. Vertical eddy-diffusion coefficients for the trace gases whose stratospheric lifetimes are given in Fig. 9.2, based on the one-dimensional formulation of Eq. (9.7.9) with a diabatic circulation similar to the equinoctial circulation of Fig. 9.15. [After Holton (1986a).]

trum to include only one or two zonal harmonic waves interacting with the zonal flow. Examples of such models as applied to purely dynamical problems appeared in some earlier chapters. In this section we consider mechanistic models applicable to various aspects of the three-dimensional transport problem; general circulation models will be discussed in Chapter 11.

One of the most enlightening mechanistic models of transport is the simplified general circulation model of Kida (1983). This model is based on the primitive equations. It includes only a single hemisphere with a wall at the equator, and has a grid resolution of 3° longitude by 2.5° latitude. There are 12 layers in the vertical, extending from the surface to the 1-mb level. Although in terms of resolution this model is similar to a typical GCM, it is here regarded as a mechanistic model because the representation of physical processes in the troposphere and the stratosphere is greatly simplified. For example, diabatic heating is given by the sum of a specified term plus a Newtonian relaxation to a specified temperature profile. There is no topography, so planetary waves are excited only by land-sea thermal contrasts.

Despite these simplifications, Kida's model does a reasonably good job of representing the Northern-Hemisphere winter circulation, including the development of upper-tropospheric baroclinic eddies. Kida used this model to analyze the long-term evolution of the position of air parcels initially located along a narrow band confined between latitudes 2.5 and 7.5°N at the 100-mb level (just above the tropical tropopause). Thus, in his experiment a three-dimensional Eulerian model is used to compute Lagrangian parcel trajectories. The long-term advection and dispersion of the initial "ribbon" of parcels is shown in the form of the parcel positions projected on the meridional plane in Fig. 9.18. The figure confirms the conceptual model of transport in the meridional plane that was introduced in Section 9.3. The parcels tend to rise in the tropics and sink at extratropical latitudes due to the diabatic circulation. But superposed on the slow diabatic drift there is a quasi-horizontal meridional dispersion that is very rapid just above the tropopause. Also indicated clearly is the preferred region of return flow from stratosphere to troposphere associated with the tropospheric subtropical jetstream. Although the model cannot resolve the actual scale of upper-level fronts and tropopause folds, it nevertheless shows that such processes are at least crudely reflected in the parcel trajectories. The overall meridional dispersion rate calculated in this model is probably an underestimate of the actual rate in the "surf zone" of the winter hemisphere because the planetary wave activity is less than observed. However, the model does provide vivid confirmation of our overall view of transport in the meridional plane.

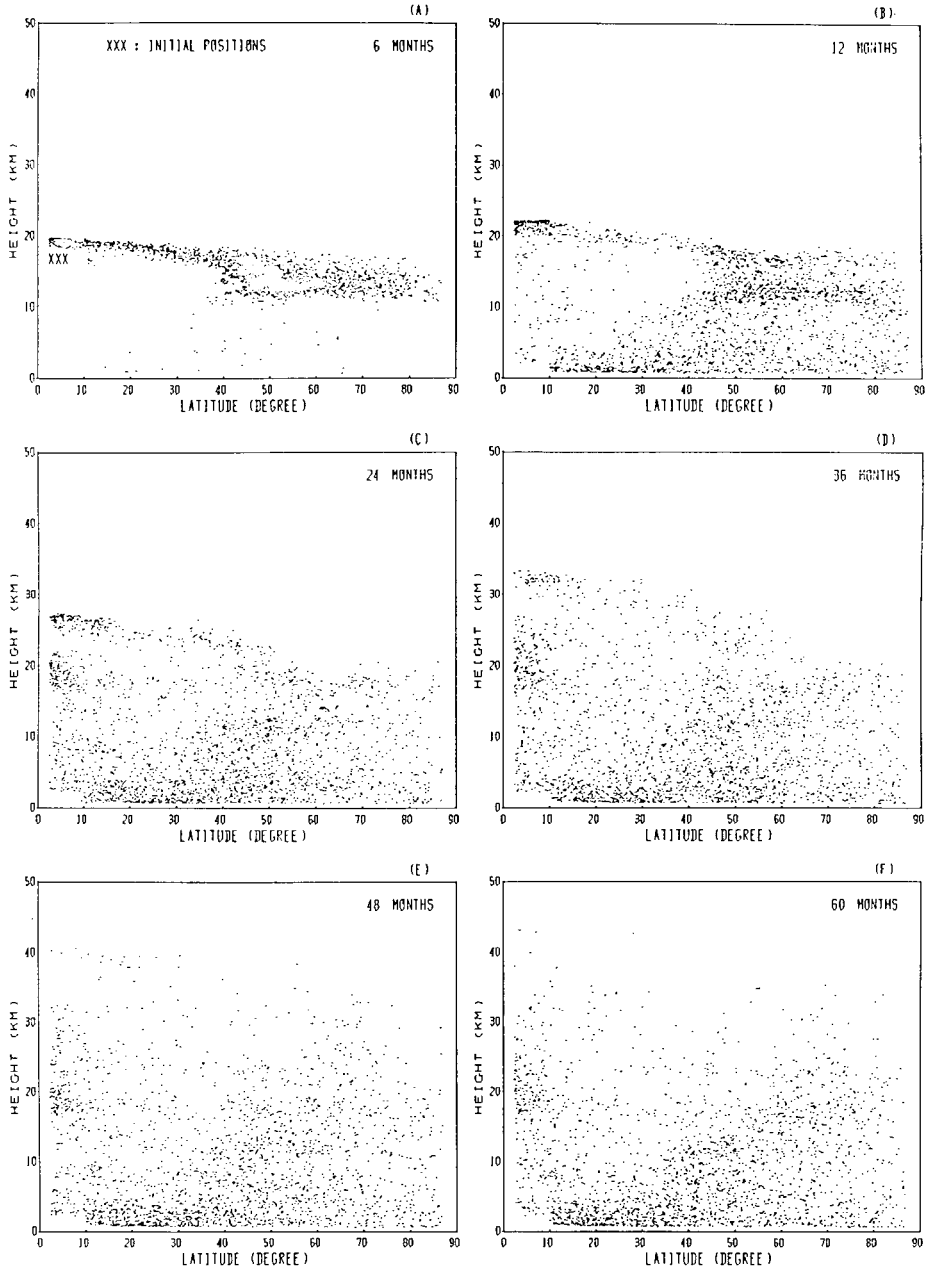

Fig. 9.18. The long-term evolution of the positions as projected on a meridional plane for air parcels originally located along a zonal band as marked by the XXX in frame (A). [After Kida (1983).]

Rapid meridional transport by planetary waves has been studied with the aid of mechanistic models that are much cruder than Kida's model. Typically such models resolve only one or two zonal harmonic waves in longitude, but retain fairly high resolution in the latitudinal and vertical direction. These models can to some extent simulate the meridional advection and zonal stretching of "tongues" of tracer associated with planetary wave breaking, of the sort pictured in Figs. 5.6 and 9.6 for the examples of potential vorticity and methane mixing ratio. However, the nonlinear cascade of tracer variance towards higher zonal wave numbers obviously cannot be simulated by such models. Despite this important defect, the Lagrangian parcel motions in such models during the evolution of simulated sudden stratospheric warmings are quite instructive.

Figure 9.19 shows an example for a simulated wave-number 1 sudden warming from the model of Hsu (1980) (see Section 6.3.2). As the anticyclonic disturbance amplifies, the air parcels that are initially evenly distributed around the 30°N latitude circle are drawn poleward and eastward around the northern flank of the high, and equatorward and westward around the southern flank. As the warming develops the parcels are advected in a narrow tongue across the polar region and are gradually "wrapped up" around the anticyclone. When viewed in the meridional plane (Fig. 9.20), the parcel evolution indicates a rapid meridional dispersion and a pronounced downward advection in the polar region. The latter is not due to the diabatic circulation (radiative effects are weak in this model), but rather represents the adiabatic downward displacement of isentropic surfaces in the polar region as a result of the sudden warming. The large vertical range of parcels in high latitudes reflects the strong longitudinal variation in vertical velocity (and temperature) associated with the wave disturbance. (Figures 9.19 and 9.20 should be compared with Figs. 6.10 and 6.11, which are for a wave-number 2 warming. The latter also show polar descent and meridional dispersion, but focus more on the splitting of the vortex and the high-latitude behavior of air parcels.)

This model has also been used to simulate ozone transport during a sudden stratospheric warming (Jou, 1985). For this purpose a very simple linear photochemistry was employed and the model-derived velocity fields were used to solve for the evolution of the ozone mixing ratio using the three-dimensional ozone continuity equation, but retaining the same zonal truncation—the zonal mean plus a single wave-number 1 disturbance. The model, despite its severe zonal truncation, was able to simulate the poleward and eastward advection of ozone-rich tongues of air, as was observed during the 1979 warming (see Section 9.5). These results suggest that sudden warmings may contribute a rather large fraction of the total poleward tracer transport during the winter season, and hence may introduce subseasonal

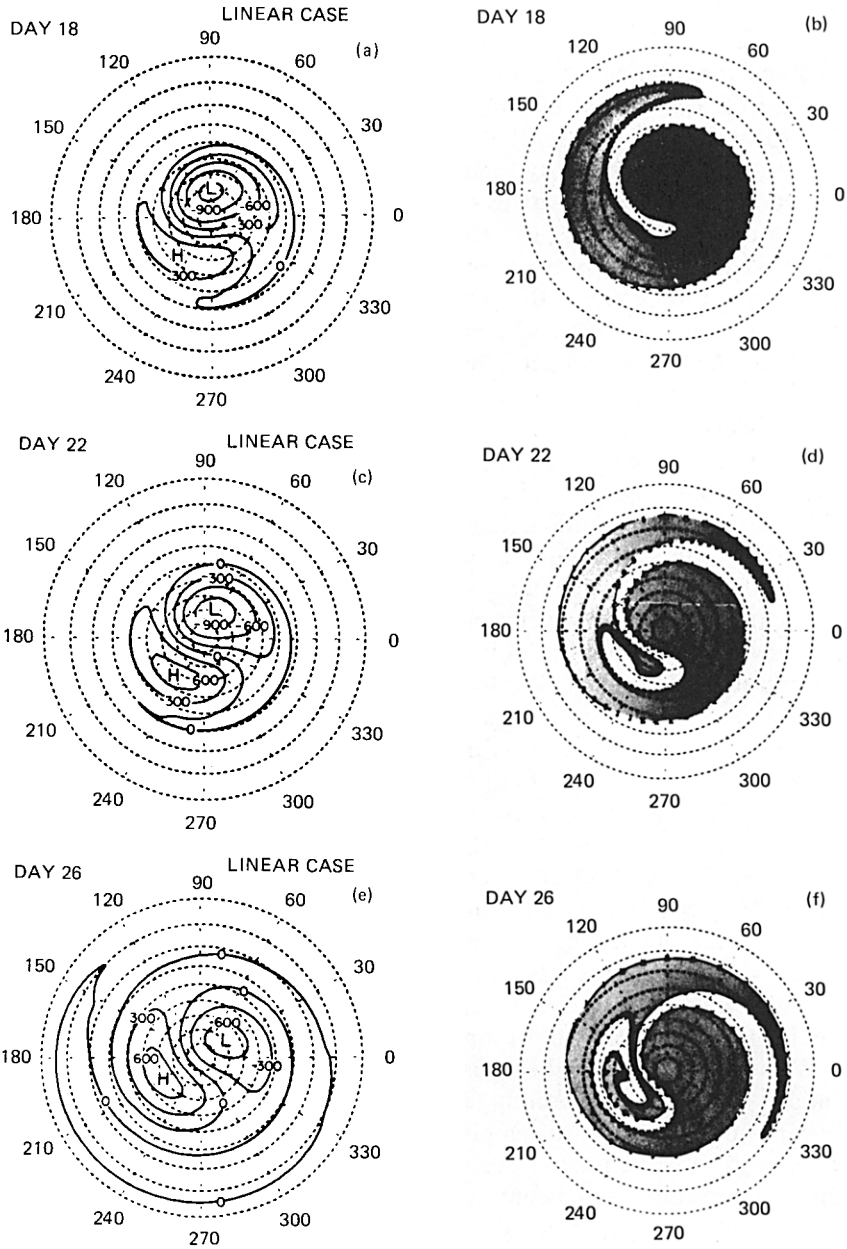

Fig. 9.19. Parcel motions during a simulated sudden stratospheric warming in a quasi-linear model in which a forced wave-number 1 disturbance interacts with the zonal flow. The left-hand frames show the evolution of the geopotential field at the log-pressure altitude $z = 30$ km. The right side shows the projection on the $z = 30$ km surface of the positions of a set of marked parcels that were initially spaced uniformly along the 30°N latitude circle. Air that was originally poleward of 30°N is shown by shading. [After Hsu (1981). American Meteorological Society.]

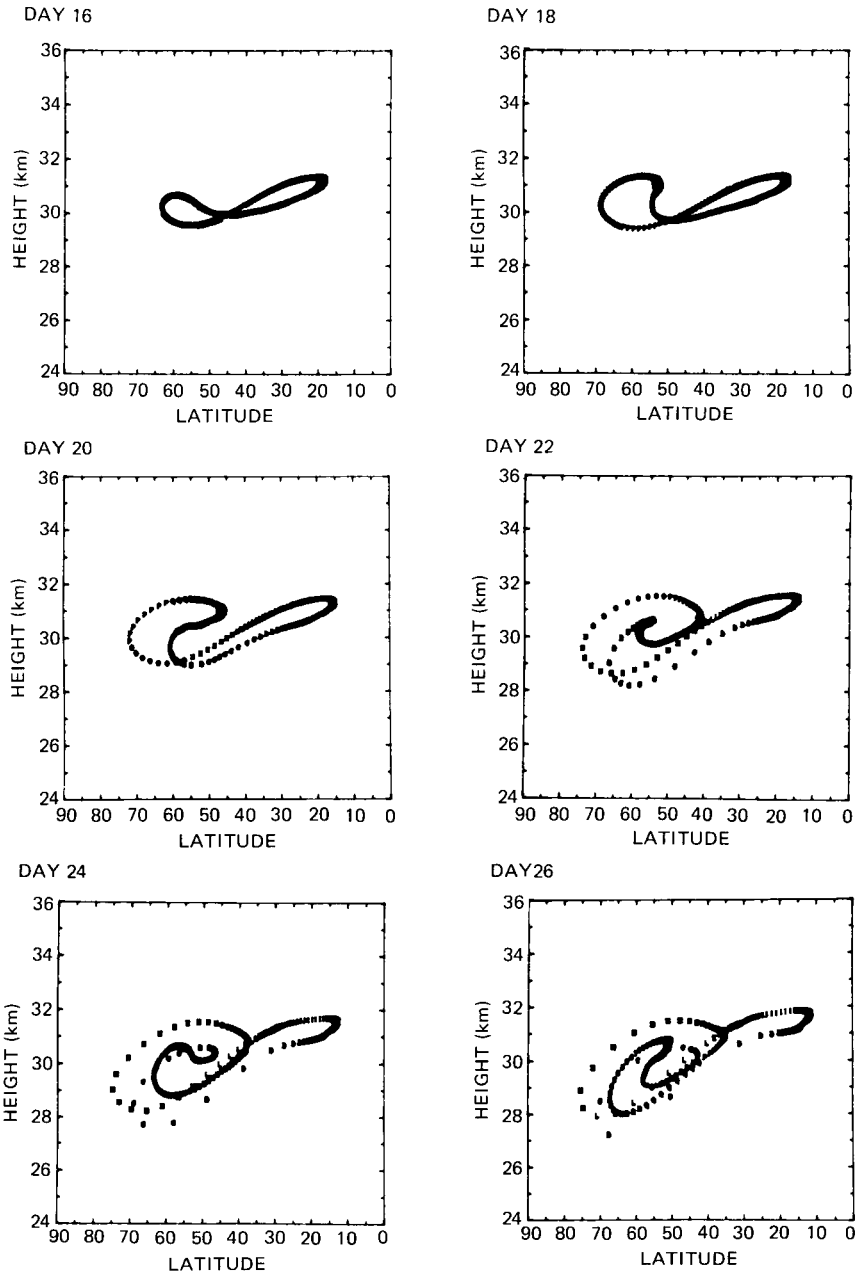

Fig. 9.20. As in the right-hand panels of Fig. 9.19, but parcel projections onto the meridional plane. Note the poleward and downward drift associated with the downward displacement of the isentropes during the sudden warming. [After Hsu (1981). American Meteorological Society.]

changes in the meridional distribution of tracers that may be difficult to incorporate in two-dimensional models.

Appendix 9A The Transformed Eulerian-Mean Transport for Small-Amplitude Eddies

For linear disturbances the components of the TEM eddy flux vector, **M**, that appear in Eq. (9.4.13) can be expressed in terms of eddy transience and departures from adiabatic and conservative motions. We express the eddy tracer perturbation as in Eq. (9.4.6) and by analogy to Eqs. (9.4.4) and (9.4.6) we let

$$\bar{D}\theta' + \mathbf{u}' \cdot \nabla\bar{\theta} = Q' + O(\alpha^2), \tag{9A.1}$$

so that with the aid of Eq. (9.4.5a),

$$\theta' + \boldsymbol{\xi}' \cdot \nabla\bar{\theta} = q'. \tag{9A.2a}$$

where

$$\bar{D}q' \equiv Q'. \tag{9A.2b}$$

Then by direct substitution from Eqs. (9.4.6) and (9A.2a) into the following definitions of $M^{(y)}$ and $M^{(z)}$:

$$M^{(y)} \equiv -\rho_0(\overline{v'\chi'} - \overline{v'\theta'}\bar{\chi}_z/\bar{\theta}_z),$$

$$= \frac{\rho_0}{\bar{\theta}_z}\left\{\overline{[v'(q'\bar{\chi}_z - \gamma'\bar{\theta}_z)]} + \tfrac{1}{2}(\overline{\eta'^2})_t\frac{\partial(\bar{\chi}, \bar{\theta})}{\partial(y, z)}\right\} + O(\alpha^3); \tag{9A.3a}$$

$$M^{(z)} \equiv -\rho_0(\overline{w'\chi'} + \overline{v'\theta'}\bar{\chi}_y/\bar{\theta}_z),$$

$$= -\frac{\rho_0}{\bar{\theta}_z}\{(\overline{w'\gamma'}\bar{\theta}_z + \overline{v'q'}\bar{\chi}_y)\} + \frac{\rho_0}{2\bar{\theta}_z}[\overline{(q' - \theta')(\gamma' - \chi')}]_t + O(\alpha^3). \tag{9A.3b}$$

Note that $\mathbf{M} = 0$ if the disturbances are linear, steady, adiabatic ($q' = 0$), and conservative ($\gamma' = 0$).

We now define $\Psi^* \equiv -\overline{v'\theta'}/\bar{\theta}_z$ [cf. Eq. (3.5.1)]; after some manipulation using Eqs. (9.4.9b) and (9A.1)–(9A.2), we obtain

$$\Psi - \Psi^* = \frac{1}{2\bar{\theta}_z}[\overline{v'q'} - \overline{\eta'Q'} + (\overline{\eta'\theta'})_t] + O(\alpha^3). \tag{9A.4}$$

This is a stream function for the difference between the effective transport circulation and the residual circulation. In general $\overline{v'q'} \neq \overline{\eta'Q'}$, so that the residual and the effective transport circulations are equal only when the waves are steady, linear, and adiabatic. The equality of the circulations does not, however, require that the tracer be conservative ($\gamma' \neq 0$, $S' \neq 0$).

References

9.1. The history of transport ideas is reviewed by Mahlman *et al.* (1984), who give extensive references to original literature. The use of isentropic potential vorticity maps is discussed thoroughly by Hoskins *et al.* (1985).

9.2. The chemistry of trace gases in the middle atmosphere is lucidly discussed by Brasseur and Solomon (1984), who provide much useful information on chemical timescales.

9.3. An interpretation of the Brewer-Dobson model in terms of the GLM theory is given by Dunkerton (1978).

9.4. The generalized Lagrangian mean (GLM) theory is discussed in the context of tracer transport by McIntyre (1980b). A lucid account of the theoretical basis for two-dimensional transport modeling is given by Tung (1982).

9.5. McIntyre and Palmer (1984) discuss the concept of "planetary wave breaking" and its role in irreversible transport. These ideas are applied to observational data by Leovy *et al.* (1985).

9.6. Stratosphere-troposphere exchange is reviewed by Reiter (1975). The problem of tropical exchange is reviewed by Holton (1984b). Implications of the *Nimbus* 7 LIMS water-vapor measurements for exchange are discussed by Remsberg *et al.* (1984 b).

9.7. One of the earliest two-dimensional transport models for stratospheric tracers was that of Reed and German (1965). Two-dimensional models that include the complete dynamical equations are discussed by Harwood and Pyle (1975) and Garcia and Solomon (1983). Contributions to the formulation of the eddy diffusion tensor include Plumb (1979), Matsuno (1980), Danielsen (1981), and Holton (1981). For more detailed treatment of the one-dimensional modeling approach described in Section 9.7.3, see Holton (1986a).